NASA TECHNICAL NOTE

NASA TN D-8163

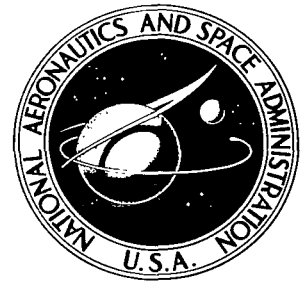

NASA TN D-8163

PERFORMANCE OF A 1.57-PRESSURE-RATIO TRANSONIC FAN STAGE WITH A SCREEN-INDUCED 90° CIRCUMFERENTIAL INLET FLOW DISTORTION

Nelson L. Sanger

Lewis Research Center
Cleveland, Ohio 44135

NATIONAL AERONAUTICS AND SPACE ADMINISTRATION • WASHINGTON, D. C. • FEBRUARY 1976

1. Report No. NASA TN D-8163	2. Government Accession No.	3. Recipient's Catalog No.
4. Title and Subtitle PERFORMANCE OF A 1.57-PRESSURE-RATIO TRANSONIC FAN STAGE WITH A SCREEN-INDUCED 90° CIRCUMFERENTIAL INLET FLOW DISTORTION		5. Report Date February 1976 6. Performing Organization Code
7. Author(s) Nelson L. Sanger		8. Performing Organization Report No. E-8218
9. Performing Organization Name and Address Lewis Research Center National Aeronautics and Space Administration Cleveland, Ohio 44135		10. Work Unit No. 505-04 11. Contract or Grant No.
12. Sponsoring Agency Name and Address National Aeronautics and Space Administration Washington, D.C. 20546		13. Type of Report and Period Covered Technical Note 14. Sponsoring Agency Code
15. Supplementary Notes		

16. Abstract

A transonic fan stage having a design pressure ratio of 1.57 was tested with a 90° circumferential distortion imposed on the inlet flow. The rotor diameter was approximately 50.8 cm, and the design pressure ratio was 1.60 at a tip speed of 425 m/sec. Overall performance at 70 and 100 percent of design speed showed (compared to undistorted inlet flow) a loss of stall pressure ratio and flow range at design speed and no significant loss in stall pressure ratio at 70 percent of design speed. Detailed flow measurements are presented to show the rotor-upstream flow interactions and the attenuation and amplification properties through the stage.

17. Key Words (Suggested by Author(s))	18. Distribution Statement
Circumferential distortion; Distortion; Transonic fan stage; Compressor	Unclassified - unlimited STAR Category 07 (rev.)

19. Security Classif. (of this report)	20. Security Classif. (of this page)	21. No. of Pages	22. Price*
Unclassified	Unclassified	74	$4.25

* For sale by the National Technical Information Service, Springfield, Virginia 22161

CONTENTS

PERFORMANCE OF A 1.57-PRESSURE-RATIO TRANSONIC FAN STAGE WITH A SCREEN-INDUCED 90° CIRCUMFERENTIAL INLET FLOW DISTORTION

by Nelson L. Sanger

Lewis Research Center

SUMMARY

A transonic fan stage was tested with a 90° circumferential distortion imposed on the inlet flow. The fan rotor was approximately 50.8 centimeters in diameter and had a 0.5 hub-tip radius ratio, a design operating tip speed of 425 meters per second, and a design pressure ratio of 1.60. Stage design pressure ratio was 1.57. Data were obtained at 70 and 100 percent of design speed. Overall performance and detailed flow parameters at three radial positions were obtained.

At design speed and near-stall flow conditions a total pressure distortion magnitude of 12 percent caused a loss in stall pressure ratio of 5 percent and also a loss in flow range. At 70 percent of design speed a lesser magnitude of distortion (4 percent) did not affect stall pressure ratio.

Significant rotor-induced interactions were observed in the upstream flow from distortion screen to rotor inlet. Total pressure distortion was relatively unaffected, but axial velocity distortion was strongly attenuated. Large tangential velocity distortions were induced in the hub region with lesser effects radially toward the tip.

Circumferential flow redistribution due to distortion tended to unload rotor blades in the undistorted sector. The resulting reduced energy addition was the primary reason for a decrease in overall pressure ratio over the operating range.

As the rotor traversed the distorted sector, varying incidence angle and tangential velocity components caused all blade elements to add energy in a circumferentially varying but significant amount. This process was accompanied by increasing losses in the distorted sector as stall was approached. Stall conditions were reached at a greater weight flow with distortion than without.

The stator blade row essentially transmitted the flow pattern generated by the rotor. However, the distorted sector was subjected to higher incidence angles and the undistorted sector to higher Mach numbers than were reached with no distortion. Higher losses were evident in the distorted sector.

INTRODUCTION

One of the principal assumptions made in designing compressors and fans is that the inlet flow is uniform and axisymmetric. In actual aircraft applications the inlet flow is quite often nonuniform (i.e., distorted) and can result in severe performance degradation. In-flight distortion of inlet flow is generally produced by aircraft attitude changes and inlet-airframe effects. Land-based turbomachinery applications can also experience distorted inlet flow conditions that are produced by upstream duct geometry.

Distortion is characterized by nonuniformity in the inlet flow parameters of velocity, pressure, temperature, flow angle, or gas constituency. Velocity, pressure, and angle nonuniformities generally result from separated boundary layer regions in the engine inlet; temperature and gas constituency nonuniformities normally occur because of engine exhaust recirculation or armament firing. Temperature distortions can also occur in latter stages of a multistage compressor that is subject only to an inlet pressure distortion. Circumferential variations in inlet flow parameters produce circumferential variations in work input, which are measured as total temperature variations.

In order to simplify analysis of the very complex patterns that are encountered, variations in the radial direction are usually considered separately from variations in the circumferential direction. Experimental tests usually are designed to produce pure radial or pure circumferential patterns. Ultimately, however, analysis of the effects of distortion must combine the effects of radial and circumferential patterns.

Distortion measurements are taken as part of a general program of research into the aerodynamics of high-performance fans and compressors conducted at the Lewis Research Center. Attention is concentrated on "steady-state" distortion patterns (magnitude and extent nonfluctuating with time) that are produced experimentally by wire mesh screens. The objective of the research is to better understand the aerodynamics of compressor flow under distorted conditions, thereby enabling more distortion-tolerant designs to be evolved.

In this report, the response of a single fan stage with a transonic rotor to a screen-induced circumferential distortion of 90° extent is presented and discussed. Detailed surveys of flow conditions at several upstream measuring stations, between the rotor and the stator, and downstream of the stator are used in the evaluation.

The subject fan stage had a design pressure ratio of 1.57 at 425-meter-per-second tip speed and was one of the reference stages for an experimental program whose objective was to determine the effect on performance of changes in selected aerodynamic and geometric design variables. Its aerodynamic performance with undistorted inlet flow is presented in reference 1. Detailed flow measurements around the circumference at three radial positions were made between the distortion screen and the rotor inlet at three axial locations. These measurements are evaluated to determine the degree of interaction between the rotor and the upstream distorted flow field. Similar detailed

flow measurements were made at the rotor and stator outlet planes to determine the stage response to the imposed distortion. Data are examined in detail at near-stall and maximum-flow conditions for design speed and at near-stall conditions for 70 percent of design speed.

APPARATUS AND PROCEDURE

The apparatus that was used in the test consisted of the single-stage fan, the test facility, the instrumentation, and the wire mesh distortion screens. A description of these items is followed by a discussion of test and calculation procedures.

SINGLE-STAGE FAN

A description of the design procedures and design details of the fan stage used in this investigation (designated as stage 11-4), as well as aerodynamic performance with clean-inlet flow, is contained in reference 1. For convenient reference the design-point overall parameters, rotor and stator blade-element aerodynamic parameters, and rotor and stator blade geometry are presented in tables I to V, respectively. All symbols are defined in appendix A. Equations and terms used in the tables are presented in appendixes B and C, respectively.

The design-point overall pressure ratio for the stage was 1.57 at a weight flow of 29.5 kilograms per second. Rotor design tip speed was 425 meters per second (about 16 000 rpm).

The rotor tip diameter was approximately 50.8 centimeters. The hub-tip radius ratio was 0.5. The nonrotating tip clearance was 0.050 centimeter, and the axial spacing between the rotor hub trailing edge and the stator hub leading edge was 3.2 centimeters. Vibration dampers having a maximum thickness of 0.21 centimeter were placed on the rotor blades at 50 percent span. The rotor was designed for a radially constant total pressure ratio of 1.60.

The blade shape for both rotor and stator was a multiple circular arc. The rotor and stator are shown in figures 1 and 2.

TEST FACILITY

The tests were conducted in the Lewis single-stage compressor facility. A schematic diagram of the facility is presented in figure 3 and a complete description in ref-

erence 2. Air enters the system through an inlet on the roof and passes through an orifice and into the plenum. It then passes through the distortion screens and the test stage into a collector, from which it is exhausted to the atmosphere. All tests were conducted with atmospheric inlet conditions. Back pressure on the stage was controlled by a slide valve located in the collector (fig. 3).

INSTRUMENTATION

Compressor flow rate was measured by using a calibrated thin-plate orifice located in the inlet piping (fig. 3). Radial surveys of the flow were made at five axial locations, three of which were upstream of the rotor. A schematic figure of the flow path and survey locations is shown in figure 4. The type of probe used to obtain the survey data is shown in figure 5 and reported in reference 3. This double-barrel probe has demonstrated ability to record accurate values of total temperature, total pressure, and flow angle.

For these distortion tests, where it was thought desirable to obtain all measurements at the same location, static pressures were obtained by averaging the pressures measured from the taps on the two sides of the 60° wedge. Calibration curves were used to relate these readings with true static pressures. Large corrections are necessary to determine true static pressure in the Mach number range $0.6 < M < 1.0$, which is the range of flow Mach numbers entering and leaving this rotor at design speed. A typical calibration curve taken from reference 3 is shown in figure 6. However, emphasis herein is placed on the change of flow conditions from undistorted flow conditions and from different flow conditions under distortion rather than on the absolute value of any single flow parameter.

Inner and outer wall static pressures were measured at rotor inlet, rotor outlet, and stator outlet stations (1, 2, and 3, respectively, fig. 4). The circumferential locations of the survey probes and the wall static pressure taps are shown in figure 7. The survey probe downstream of the stator (station 3) was circumferentially transversed one stator blade passage (7.5°) in nine steps counterclockwise from the position shown in the figure.

All pressures were transmitted through a Scanivalve system and measured by calibrated transducers. Rotor rotational speed was measured by an electric speed counter, which sensed pulses from a magnetic pickup.

The estimated errors based on inherent accuracies of the instrumentation and recording system are

Weight flow, kg/sec	±0.3
Rotative speed, rpm	±30
Flow angle, deg	±1
Temperature, K	±0.6
Rotor inlet total pressure, N/cm^2	±0.01
Rotor outlet total pressure, N/cm^2	±0.10
Stator outlet total pressure, N/cm^2	±0.10
Rotor inlet static pressure, N/cm^2	±0.04
Rotor outlet static pressure, N/cm^2	±0.07
Stator outlet static pressure, N/cm^2	±0.07

Figure 8 permits data accuracy to be approximated for circumferential distortion data. Integrated weight flow at each station is compared to orifice weight flow. Upstream flow measurements indicate the most accuracy, and the rotor outlet station the least. The figure is more an approximation of overall performance data accuracy than a presentation of detailed data since integrated values are used in the comparison and the integration is performed over only three radial positions.

DISTORTION SCREENS

The distortion screen assembly used in the investigation was located 36.25 centimeters upstream of the rotor hub leading edge. It was rotated to 12 circumferential positions to obtain the distortion patterns measured by the single survey probe. Trial and error tests were conducted to determine the screen extent that would produce a consistent 90° circumferential distortion pattern over the blade span at the rotor inlet. The resulting screen covered 85° at the tip and 135° at the hub diameter. A 20×20 wire mesh (8 wires/cm, or 20 wires/in.) was used. Wire diameter was 0.051 centimeter, resulting in a 36 percent open area. It was secured to a backup screen having a 1.9-centimeter by 1.9-centimeter clear opening and a 0.27-centimeter wire diameter. Support struts (8 in number) for the backup screen were streamlined such that the cross section resembled an ellipse having a maximum thickness of 0.76 centimeter. The screen assembly is shown in figure 9.

TEST PROCEDURE

With only the backup screen (BUS) in place, radial surveys were taken over a range of weight flows (obtained by adjusting back pressure on the stage) from maximum flow to near-stall conditions at 70 and 100 percent of design speed. At 60, 80, and 90 percent

of design speed, surveys were taken only at the near-stall weight flow. Data were recorded at 11 radial positions for each speed and weight flow. At each radial position the combination probe behind the stator was traversed circumferentially in nine steps across the stator gap (7.5°).

At each speed the back pressure was increased by closing the outlet valve until a stall condition was obtained. Stall conditions were indicated by a sudden drop in stage outlet pressure (measured by a midpassage monitoring probe and recorded on an X-Y plotter), by large increases in measured blade stresses on both rotor and stator, and by a sudden increase in audible noise level. Radial survey data were taken at a weight flow as close to actual stall as practical. In general, this was within 0.5 kilogram per second of the actual stall weight flow.

For the circumferential distortion tests, radial survey data were taken only at 100 and 70 percent of design speed. At 100 percent speed, data were taken at three weight flows: near stall, midflow, and maximum flow. At 70 percent speed, data were taken at near-stall and midflow conditions. Stall conditions were obtained as in the BUS tests.

With circumferential distortion, survey data were recorded at three radial positions: 10, 45, and 90 percent of span from the tip. A radial survey was taken at each of the 12 screen positions. At each radial position the probe behind the stator was circumferentially traversed to nine different locations across the stator gap.

At near-design flow conditions the magnitude of distortion measured at the rotor inlet midspan radial position was $(P_{max} - P_{min})/P_{max} = 0.12$.

CALCULATION PROCEDURE

All data presented in this report have been adjusted to standard conditions (total pressure of $10.13\ N/cm^2$ and total temperature of 288 K) at the rotor inlet (station 1). The term equivalent when applied to weight flow or speed refers to corrected values of these parameters. The calculation procedure used for BUS data is the same as that used for clean-inlet tests and is given in reference 1. The following discussion applies to the calculation procedure used for circumferential distortion data only.

Measured total temperature and static and total pressure were corrected for Mach number and streamline slope according to the procedure given in reference 1. Calibration curves are presented in reference 3. Before adjustment to standard conditions, circumferential distortion data were mass-averaged circumferentially and radially.

At all stations (-1 to 3, fig. 4) the following quantities were determined at each radial and circumferential position: p, P, T, β, M, V, M_Z, and V_Z (see appendix A). At station 3, wall static pressure was provided in addition to these quantities. And at the rotor inlet and outlet (stations 1 and 2), M', V', β', and wall static pressure were

also calculated. No blade-element performance parameters were calculated because of the asymmetric nature of the flow, which, in the rotor relative flow plane, is unsteady. For the same reasons the data were not translated from the measuring station to the blade edge planes.

Downstream of the stator (station 3) a circumferential traverse of a single blade passage was made in nine steps to obtain measurements of pressure, temperature, and flow angle. The nine values of total temperature were mass averaged to obtain a single value for total temperature at the stator outlet. This mass averaging was done for each of the points corresponding to the 12 screen positions. The nine values of total pressure were converted to their enthalpy equivalent ($PR^{(\gamma-1)/\gamma} - 1$) and then mass averaged. From the nine measured values each of total pressure, total temperature, and flow angle, corresponding values of axial velocity and tangential velocity were computed. These velocities were mass averaged and a single value for flow angle obtained. Thus, single values for pressure, temperature, and flow angle at the stator outlet were calculated at each of the 12 screen positions.

In order to obtain overall total temperature and pressure ratios, the 12 circumferential values were mass averaged. Integrated weight flow was computed at each station based on radial survey data.

For axisymmetric flow, as reported in reference 1, 11 radial positions are used in the averaging process. Backup screen data were reduced and are presented in this manner herein. However, when BUS and circumferential distortion overall performance data are compared directly in this report, only the three radial positions corresponding to those taken for distorted flow are used in the averaging process for BUS data. Therefore, some small difference between overall performance figures presented herein may be noted.

RESULTS AND DISCUSSION

The results from this investigation are presented in two main sections. Performance without circumferential distortion screens but with the backup support screen in place are presented first. This constitutes the reference condition from which circumferential distortion effects are determined. The second main section discusses performance under circumferentially distorted flow conditions.

REFERENCE CONDITION: BACKUP SCREEN TESTS

Overall Performance

The overall performance for rotor 11 and for stage 11-4 with the backup screen in

place is presented in figure 10. Data at 11 radial positions were mass averaged to obtain the values shown in the figure. Data at several weight flows from maximum flow to near stall are presented for 70 and 100 percent of design speed. For 60, 80, and 90 percent of design speed, performance is presented at the near-stall condition only. Design-point values are shown as solid symbols. Stall lines were determined by using the method described in the section TEST PROCEDURE.

At the design weight flow of 29.5 kilograms per second the experimental stage pressure ratio and the total temperature ratio were 1.54 and 1.16, respectively. The experimental peak efficiency of 0.83 was 3 points less than design value. Stall margin at design speed was 18 percent based on weight flows and stage total pressure ratios at peak efficiency and at stall.

Radial Distributions of Performance Parameters

The radial distributions of selected flow and performance parameters at design speed are shown in figure 11 for the rotor and in figure 12 for the stator. The data shown represent the flow conditions at near stall, peak efficiency, and maximum flow. Design values are shown by solid symbols. For this case only, the data shown have been translated to the blade leading and trailing edges.

A general condition that can be observed at all operating points is the noticeable effect on the profiles of the rotor damper in both rotor and stator performance.

An operating point of particular interest is the near-stall point. Inspection of the figures shows that no single region of the rotor or stator can be identified to be critical but that the blade damper and end-wall areas show the highest losses and blade loading (diffusion factor, D). Table VI summarizes the state of key blade-element parameters near stall at design speed.

PERFORMANCE WITH CIRCUMFERENTIAL DISTORTION

Overall Performance

The overall performance for rotor 11 and stage 11-4 with a 90° circumferentially distorted inlet flow is presented in figure 13. For comparison the data without distortion (BUS) are also plotted. The distortion data are presented at three weight flows for design speed (near stall, midflow, and maximum flow) and at two weight flows for 70 percent of design speed (near stall and maximum flow). Rotor and stage performance show similar trends, so this discussion is confined to stage performance (fig. 13(b)).

It should be recalled that overall performance is calculated by mass averaging appropriate parameters over the radial height of the passage. For undistorted flow, this mass averaging was done over 11 radial positions, which provided a highly accurate measure of performance. However, only three radial positions were measured for circumferentially distorted flow. In order to provide a basis for comparison, the BUS performance was therefore recalculated for three radial positions. These values are used in figure 13.

Some efficiency values for the circumferential distortion case appear abnormally high and should be disregarded. Efficiency (eq. (B9)) is extremely sensitive to small differences in pressure or temperature. For example, with the stage design-point values as a reference, a change in pressure ratio of 2 percent, with no change in temperature ratio, produces a 4-point (4.7 percent) change in efficiency. With pressure ratio held constant, a change of 2 percent in temperature ratio produces a 10.7-point (12.5 percent) change in efficiency. In view of the circumferential and radial averaging process and the small number of radial measuring positions, small differences can occur whose influence on efficiency are quite large.

The primary effects of distortion occur at design speed. At this higher speed the flow rate is greater, the pressure drop across the screen is greater, and the corresponding distortion magnitude is greater. Defining the magnitude of distortion as $(P_{max} - P_{min})/P_{max}$ taken circumferentially at a constant ring diameter r/r_t of 0.45, the magnitude is 12 percent at design speed and 4 percent at 70 percent of design speed (both near-stall points). At design speed the pressure ratio, operating flow range, and stall margin were reduced. (The stall line was moved to higher flows as compared to undistorted flow.) At 70 percent of design speed, stall margin was not affected.

From the near-stall points at design speed for undistorted and distorted flow (fig. 13(b)), the stage pressure ratio was reduced by distortion from 1.64 to 1.56. One means of quantifying the effect of distortion on stall performance is to evaluate the loss in the stage stall-pressure-ratio parameter (eq. (B18)), $\Delta PRS = 1 - (PR_{d,s}/PR_{u,s})$, evaluated at constant equivalent speed. At design speed this loss is equivalent to 5 percent, based on the pressure ratio at the measured near-stall points.

Rotor-Upstream Flow Interactions

Previous investigators have observed that there is interaction between a rotor and a nonuniform upstream flow field. Analytical and supporting experimental studies (refs. 4 to 7) have shown that - as flow moves from screen to compressor - total pressure defects are unchanged, axial velocity defects are reduced, and tangential and radial components are induced into the flow in the region upstream of the rotor. Of the analytical

studies, all have included one or more limiting assumptions such as incompressible flow, two-dimensional flow field, small perturbations, or rotor-alone cases. All experimental work has been restricted to incompressible flow or low subsonic studies. The data presented herein are from a modern, transonic, highly loaded fan with a low hub-tip radius ratio.

In this section, detailed data are presented at three upstream axial locations in order to document the rotor - upstream flow interactions. The upstream stations are designated -1, 0, and 1 (fig. 4) and are at 0.71, 0.45, and 0.05 diameter upstream of the rotor hub leading-edge plane, respectively. The data are presented at each station for three radial positions, which allows a first estimate of both the radial variations and equilibrium adjustments to be made. Two flow conditions are considered, the near-stall and maximum-flow points, both at design speed.

Presented in figure 14 are total and static pressures and axial and tangential velocity distributions for the near-stall flow point. For each radial location the distribution of each parameter is shown at stations -1, 0, and 1. Little change occurs in total pressure with axial distance (except for mixing at the edges of the shear layer between distorted and undistorted flow). But changes do occur in each of the other parameters. Axial velocity tends to become more uniform as the flow approaches the rotor, while static pressure, initially almost uniform, becomes distorted. There is initially very little swirl (tangential velocity) in the flow at station -1. But a large amount of swirl, both corotating and counterrotating, has been induced by the time the fluid reaches station 1.

The only parameter to show strong three-dimensional effects is the absolute tangential velocity. The induced swirl is much stronger near the hub than near the tip. The distribution of incidence angle at the rotor inlet is shown in figure 14(d) for the three radial positions. Because of the combination of large induced tangential velocity, low axial velocity, and low blade speed, the range and maximum value of incidence angle at the hub exceed those at the other radial positions. In the screen "shadow" region, the incidence angle at all radial positions exceeds the angles measured at stall with undistorted flow (solid symbols, fig. 14(d)).

The interaction effects are shown much more graphically for each of the parameters in the series of contour maps (fig. 15). The contour maps are generated by linear interpolation between known input points (ref. 8).

The same series of parameters are plotted in figures 16 and 17 for the maximum-flow point. Similar trends are evident, which indicates that there are no significant changes in flow mechanism over the operating flow range of the fan.

The foregoing effects are summarized in figure 18, which describes the amount of attenuation or amplification of the distortion at each radial position. The magnitude of the distortion at each station is referenced to the magnitude at station -1, just behind the

screen. The magnitude is measured as the defect in each parameter in the distortion region (maximum minus minimum) divided by the maximum value. The induced tangential velocity is referenced to the defect in axial velocity at station -1. The magnitude of tangential velocity is the magnitude greater or less than zero (V_θ distributions approximately symmetrical). The trends with flow rate are similar for each parameter, the only difference being a slightly stronger effect on each parameter at the higher flow rate. At the near-stall condition, total pressure distortion is attenuated to about 95 percent of initial distortion; at maximum flow it is attenuated to about 90 percent. In either case, the effect on total pressure distortion is relatively weak, but axial velocity distortion is strongly attenuated to about 60 percent of initial distortion (near-stall flow). Tangential velocity change due to distortion, as a percentage of initial axial velocity defect, is strongly amplified in the hub region to 75 percent of the initial axial velocity defect for near-stall flow and 85 percent for maximum flow. For either flow condition the tip region shows amplification to only about 30 percent. Static pressure distortion is also amplified, as shown in figure 18.

In representing the magnitude of a distorted flow field it is quite common to describe it in terms of the total pressure distortion at the fan or compressor face. However, because of the interaction effects between the rotor and the upstream flow, total pressure parameters may not be sufficient to describe the distortion meaningfully. Certainly, the attenuation of axial velocity distortion and the amplification of tangential velocity components will have important effects on velocity triangle relations and incidence angles.

Circumferential Flow Distributions

Conventional compressor data analysis is established on the premise of steady, axisymmetric inlet and outlet flow conditions. When the inlet flow is circumferentially distorted, some important compressor parameters cannot be accurately calculated or evaluated

(1) Because the rotor relative flow field is unsteady

(2) Because matching an outlet condition to its corresponding inlet condition is uncertain

Blade-element parameters such as diffusion factor, loss coefficient, meridional velocity ratio, and efficiency are therefore not available. Because of the unsteady relative flow field, they are probably also not applicable. Data analysis is consequently directed toward behavior of selected parameters measured or calculated at each axial station, rather than between two stations.

Where applicable, the values of parameters measured in undistorted flow (backup

screen tests, BUS) are noted on the figures. One measure of the severity of the distortion is the amount by which the corresponding undistorted value is exceeded in the distorted sector, and another is the circumferential extent over which the excursion occurs. Significant divergences from the undistorted values are noted in the following discussion.

Three operating conditions are considered: the near-stall condition at 100 percent of design speed, the maximum-flow condition at design speed, and the near-stall condition at 70 percent of design speed.

Near stall at design speed. - Presented in figure 19 are circumferential distributions through the stage of the following parameters for the near-stall point at design speed: total and static pressure, axial velocity, total temperature, incidence angles, flow angles, and inlet Mach numbers. Included on each figure as solid symbols are the near-stall conditions for undistorted inlet flow (BUS). Figure 19 is of interest principally for two reasons: (1) because it illustrates how different sections of the rotor blade span respond to unsteady (relative) inlet flow, and (2) because it represents flow conditions very close to flow breakdown due to stall.

Several observations can be made from these data. As noted earlier, all blade elements are subject to circumferential variations in incidence angle, with the largest occurring in the hub region and the smallest in the tip region. These variations are caused by the combination of axial velocity, induced tangential velocity, and blade speed in the respective regions. Variation in incidence angle implies a change in loading and in energy addition, although it can be tempered by axial velocity changes across the blade row. An increase in rotor incidence angle gives a larger expansion in the forward portion of the blade suction surface, which leads to higher suction-surface Mach numbers and stronger shocks.

The distributions of total pressure and temperature (figs. 19(a) and (c)) show that the tip region demonstrates a more direct response to distortion than do the other regions. The more direct response to a change in flow conditions that is characteristic of the tip region is commonly observed in axisymmetric flow (fig. 11). The difference in response is due to the higher stagger angles and relative velocities in the tip region. The general tendency of direct tip-element response to off-design excursions normally makes the tip region the most likely critical site for stall initiation. However, the data presented herein do not show clear evidence of stage stall occurring at any blade element. The difference in the response of blade elements along the blade span, in addition to requirements that radial equilibrium be satisfied, illustrates the difficulty of analyzing or predicting the condition of the flow by using measurements at only a single radial position or even by using a radial average.

The unsteady response of the rotor blade to a circumferentially distorted inlet flow can probably best be illustrated by comparing figures 19(a) and (c). Total temperature is a measure of energy addition, and in figure 19(c) it is seen to increase as the rotor

enters the distorted sector (circumferential location, 135°). It exceeds the total temperature level associated with stall for BUS flow at a circumferential location of about 180° for all blade sections. Outlet total pressure (fig. 19(a)) follows the temperature trend to 180°. Beyond this circumferential location the temperature continues to increase (energy continues to be added), but total pressure decreases. This implies that losses are increasing rapidly, presumably as a result of boundary layer separation (a local blade stall but not a general compressor stall). The correspondence in circumferential location of total pressure breakdown and temperatures exceeding BUS levels should be noted. Any general significance must await analysis of data from other stages. After the rotor passes through the distorted sector, the pressure recovers, indicating that the boundary layer has reattached. This effect can clearly be identified at the tip and mean sections but not necessarily at the hub. Some other mechanism such as radial equilibrium or some mechanism associated with blade solidity may be controlling behavior in the hub region.

The unsteady behavior exhibited by the rotor blade is analogous to the dynamic stall behavior observed in oscillating airfoils (ref. 10). The mechanism is considerably more complex in a compressor rotor because of blade twist and end-wall boundary layer interaction effects.

The distribution of parameters at the stator outlet reflects the influence of several factors that cannot easily be separated. Total pressure distributions reflect the combined effect of rotor energy addition in an unsteady relative flow field and losses sustained in both rotor and stator blade rows. In addition, total pressure and axial velocity together must reflect adjustments necessary to satisfy the downstream boundary condition of constant static pressure. The low axial velocity in the stator hub region (140° to 180°) constitutes a potential critical flow region to some downstream component, whether it be a second-stage rotor or the core compressor.

The static pressure distributions (fig. 19(a)) at the stator outlet are consistent with the residual flow angularity (fig. 19(d)) and indicate that some adjustment is still necessary between the stator outlet measuring plane and the downstream boundary condition of constant static pressure.

The passage of the rotor through the distorted sector is an unsteady flow phenomenon. The stator, however, operates in the absolute flow plane and sees a steady flow. Some stator blades always operate in the distorted sector; others always operate in the undistorted flow. The plot of stator incidence angle (fig. 19(f)) shows that most stator blades were operating at incidence angles less than the value measured at near stall in undistorted flow. It is also interesting to note from figure 19(g) that circumferential distortion tends to increase the stator inlet Mach number in the undistorted sector because of the circumferential redistribution of flow. The effect is strongest in the hub region, which also tends to be the highest loaded stator blade section.

A representation of stator losses can be obtained from figure 20, which shows total pressure distributions at stator inlet and outlet stations for each blade element. The distance between the curves represents losses; at all blade elements, differences are greatest in the distorted sector (where incidence angle was greatest). In general, the tip element appears to have slightly higher overall losses than the hub. The generally low incidence angles and apparently well-behaved losses do not indicate the stator to be a problem area.

An indication of the attenuation or amplification properties of each blade element is provided by figure 21. A measure of distortion magnitude is the ((Maximum - Minimum)/Maximum) parameter for pressure and velocity, which is evaluated around the circumference and at a constant radius. The station 1 value is a reference value. Magnitudes greater than those at station 1 are considered to be amplified, and magnitudes less than those at station 1 are considered to be attenuated.

It is clear, as previously noted, that the hub element amplifies the distortion (total pressure and axial velocity) mainly through the rotor. Other blade elements either produce no change in magnitude or slightly attenuate the distortion. The static pressure distribution, although tending toward uniformity, does not yet achieve it at the stator outlet measuring station. And a temperature distortion is introduced that varies radially as well as circumferentially.

Although this stage was tested with circumferential distortion only, it is worth noting that a natural occurrence of operation at off-design conditions (with or without distortion) is the introduction by the rotor of what might appear to be a radial distortion. That is, with uniform inlet flow, but at off-design conditions, the response of rotor blade elements and the requirements of radial equilibrium produce radial distributions of flow that differ from design-point distributions. (Stage 11-4 was designed for radially constant total pressure.) If evaluated with a radial distortion parameter ((Maximum - Minimum)/Maximum), such conditions would produce finite values of the parameter even though the flow was not initially distorted. Such values are shown as solid symbols in figure 22 for the near-stall condition (BUS). (A very small amount of true radial distortion was present at the inlet as indicated by the value of 0.02 at station 1.) If radial distortion tests were then to be conducted at this flow condition, the resulting radial distortion parameter would be compared to the BUS parameter, since BUS tests represent clean-inlet, off-design reference values.

Test results for near-stall operation with circumferential distortion are also plotted in figure 22 for each circumferential position of the screen. The figure illustrates the complexity of the response of the stage. The value of the radial distortion parameter varies circumferentially, being higher than BUS values behind the screen and lower in the undistorted sector. It is clear that in responding to the circumferential distortion the stage introduced a radial distortion that was not present in the BUS tests.

The resulting flow pattern is shown graphically in figure 23. It should still be recognized that part of the radial variation indicated is due to true off-design operation and part to rotor response to circumferential distortion. The flow condition portrayed corresponds to data presented in figure 15(a).

Maximum flow at design speed. - Circumferential distributions of total temperature, flow angle, rotor incidence angle, rotor and stator absolute Mach number, and rotor inlet relative Mach number are plotted in figure 24 for the maximum-flow condition at design speed.

The magnitude of distortion is greater than at near-stall conditions because the flow rate is greater, which results in a larger pressure drop across the screen. At rotor inlet the hub region shows the greatest range of incidence angle in the distorted sector (-8.5° to 5.5°). At the rotor outlet, the total temperature distributions follow incidence angle closely. The rotor response does not demonstrate quite the same dynamic effect as at near-stall flow. Because there is less energy added in the distorted sector and no strong boundary layer separation is indicated, the distortions (both total pressure P and axial velocity V_z) are not attenuated (fig. 24). This results in the distortions in P and V_z being effectively transmitted as deficits. The rotor hub section amplified total pressure and axial velocity distortions and introduced the greatest amount of temperature distortion. At the stator outlet, some nonuniformities in angle remain and are reflected in the outlet static pressure distributions.

The plot of total pressure at stator inlet and outlet stations (fig. 25) shows that stator losses are relatively low in the hub region. The higher losses in total pressure at tip and mean elements are probably partly due to elevated (over BUS values) stator inlet absolute Mach numbers. The attenuation and amplification plots (fig. 26) show the rotor hub region to be the location for the greatest amplification of distortion. A small amount of amplification through the stator mean and tip elements is indicated.

In summary, at maximum-flow conditions, the distortion produced the greatest range of rotor incidence angle excursion in the hub region. The rotor hub element amplified both total pressure and axial velocity distortion. The stator hub essentially transmitted the distortion without either ampliflying or attenuating it. Other sections of rotor and stator blade span had lesser effects on the distortion.

Near stall at 70 percent of design speed. - Circumferential distributions of total and static pressure, axial velocity, total temperature, flow angle, incidence angle, and rotor inlet relative Mach number are plotted in figure 27 for the near-stall condition at 70 percent of design speed.

The inlet total pressure distortion is quite small, only 4 percent at midspan ((Maximum - Minimum)/Maximum), because of the low flow rate at 70 percent of design speed. However, absolute flow angle showed a sizable excursion, and inlet axial velocity distortion was as large as 23 percent at midspan despite the low velocity level of 90 to 110 meters per second.

Relatively strong effects were observed in both hub and tip regions. At the hub, rotor incidence angle showed a greater excursion than at other blade elements in the distorted sector. Hub total pressure and axial velocity demonstrated the same large increase at the trailing edge of the distorted region as was observed previously at the near-stall conditions for design speed.

In the tip region a large increase in total temperature in the rotor distorted sector was observed. Almost no increase in total pressure occurred. This is essentially the same phenomenon that was observed in the tip region at near stall for design speed. It suggests a blade boundary layer separation (airfoil stall) with subsequent recovery (after passing the screen) and/or a local region of high losses. Coupled with this is the appearance of a deficit in axial velocity at the tip centered around 240° (station 2). This low axial velocity, combined with the large wheel speed component, produces a large absolute velocity component and a correspondingly large absolute flow angle. The large absolute flow angle accounts for the very large stator incidence angles indicated in the tip in figure 27(f) and the larger total pressure losses inferred from figure 28.

The attenuation and amplification plot (fig. 29) shows no large attenuation or amplification of total pressure distortion. Axial velocity distortion is amplified only through the rotor and at both hub and tip elements.

It is difficult to positively identify a critical stall site for this flow condition, although the rotor tip is the most likely location. However, the question of stall initiation with distorted flow was not of as great an interest at this speed since no loss in stall margin from undistorted flow conditions was indicated.

GENERAL DISCUSSION

In reviewing the detailed results, certain general observations can be made regarding the response of this stage to a circumferentially distorted flow and the problems inherent in modeling the flow.

In attempting to model a circumferentially distorted flow, it is attractive to treat the flow through undistorted and distorted sectors separately in a manner similar to the parallel compressor model (ref. 11). Such an approach neglects unsteady flow effects by using radially averaged values of parameters in each sector. This type of model can be helpful in a general way and only on an overall performance basis. For example, for the single-stage fan investigated in this report the two sectors are 270° (undistorted) and 90° (distorted) in extent. For a given operating condition and compared with clean-inlet conditions, the undistorted flow sector has a higher average axial velocity and therefore carries more flow per unit area. It also has a lower rotor incidence angle than the clean-inlet condition and consequently is more lightly loaded. Energy addition

is lower, and therefore outlet pressure and pressure ratio are lower than the corresponding clean-inlet condition.

Conversely, the distorted sector passes proportionately less flow, is more highly loaded, and adds more energy than corresponding clean-inlet conditions. Outlet total pressure is greater over a portion of the sector, but losses increase as boundary layer separation occurs.

If the two sectors are combined to obtain an estimate of overall performance, the effect of mass averaging over the respective extents produces lower (than clean inlet) levels of energy addition, outlet pressure, and pressure ratio. This type of simple two-sector analysis explains the lower overall performance obtained with circumferential distortion (i.e., the shifting downward of the constant-speed line in fig. 13).

Such a simple model is insufficient for purposes of obtaining insight into the flow mechanisms. Instead, detailed flow measurements that define the full three-dimensional, compressible flow field must be obtained and analyzed. In this report, such detailed data provided some insight into the performance of one stage. Although the extent to which it can be generalized is not known, it does form a basis for further investigations. Upstream inlet flow redistributions showed some strong three-dimensional effects, with large tangential velocity components near the hub (figs. 14 to 18). Because of higher stagger angles and blade speed the rotor tip element responded more quickly to circumferential inlet flow variations and showed an ability to add energy without amplifying the distortion (figs. 21, 26, and 29). The slower responding hub element produced the most amplification of the distortion. The response of the rotor at near-stall conditions was similar at design speed and 70 percent of design speed. A comparison of circumferential distributions of total pressure and total temperature showed a circumferential region of high losses (T increases while P does not). The response is somewhat altered at maximum-flow conditions since the blade loading is not so severe in the distorted sector.

These data and observations demonstrate the complexity of the compressor flow problem for distorted inlet conditions and form the beginning of a base upon which further detailed experimental knowledge may be built. Near-term progress will depend heavily upon systematic experimental investigations because the combination of analytical problems (e.g., unsteady, compressible, three dimensional, and nonlinear) makes the problem one of the most difficult in the field of fluid mechanics.

SUMMARY OF RESULTS

A transonic fan stage was tested with a 90° circumferential distortion imposed on the inlet flow. Distortion was produced by a wire mesh screen secured to a rotatable support screen. The fan rotor was approximately 50.8 centimeters in diameter and had

a design operating tip speed of 425 meters per second and a design pressure ratio of 1.60. Data were obtained at 70 and 100 percent of design speed. Overall performance and detailed flow parameters at three radial positions were measured. The circumferential distortion conditions were compared with each other and with measurements taken with only the support screen in place (undistorted flow). The following results were obtained:

1. A circumferential distortion of 12 percent magnitude at the midspan position was imposed on the subject fan stage at design speed. Losses in flow range and stall margin resulted. The loss in stall pressure ratio from undistorted conditions was 5 percent. At 70 percent of design speed, a lesser magnitude of distortion (4 percent) caused a reduction of flow range but did not affect stall pressure ratio.

2. Significant interaction between the rotor and the distorted flow field between the screen and the rotor was recorded at design speed. At near-stall flow and design speed, moving from screen to inlet, the total pressure distortion was essentially unaffected (only a 5 percent attenuation). Axial velocity distortion at near-stall flow was attenuated to about 60 percent of its initial value. Initially, absolute tangential velocity was practically zero. But strong components were induced in the hub region, and distortions less than half the hub values were induced in the tip region. Static pressure distortion was also amplified. Similar trends were shown at the maximum-flow condition and, except for static pressure, the effects were stronger in magnitude there.

3. At any given flow rate, circumferential distortion resulted in flow redistributions that reduced overall pressure ratio from levels obtained without distortion. The flow redistributions resulted in more flow through the undistorted sector, lowering incidence and increasing axial velocity. This tendency to unload the blades and to lower energy addition in the undistorted sector is the principal reason for the decrease in average outlet total pressure over the operating range.

4. In the distorted sector of flow the rotor experienced a large increase in energy addition (total temperature), which, at near-stall conditions, exceeded the levels measured with no distortion. Comparison of total temperature and total pressure distributions showed a region in the distorted sector where total pressure decreased while total temperature continued to increase. This was interpreted as a region of loss caused by a blade-surface boundary layer separation, a dynamic effect that occurs periodically once per revolution as the blade transverses the distorted sector. Similar behavior was noted for near-stall operation at 70 percent of design speed. At the maximum-flow condition (design speed) this dynamic effect was much less prominent.

5. The stator responded to the distorted flow distribution from the rotor by essentially transmitting it without significant change. Circumferential flow redistribution caused by the screen resulted in higher flow through the undistorted sector. This produced higher stator inlet Mach numbers in that sector than were measured with no dis-

tortion. Locally large incidence angles occurred in the distorted sector, and higher losses were recorded there.

6. The ability of the rotor and stage to attenuate the distortion was dependent on radial position. The rotor hub amplified pressure and velocity distortions at all flow and speed conditions tested. Tip and mean elements did not substantially change distortion magnitude. At each radial position the rotor introduced a significant temperature distortion. The stator did not display strong amplification or attenuation properties.

Lewis Research Center,
National Aeronautics and Space Administration,
Cleveland, Ohio, October 14, 1975,
505-04.

APPENDIX A

SYMBOLS

A_{an}	annulus area at rotor leading edge, 0.147 m^2
A_f	frontal area at rotor leading edge, 0.198 m^2
C_p	specific heat at constant pressure, 1004 J/(kg)(K)
c	aerodynamic chord, cm
D	diffusion factor
g	acceleration of gravity, 9.81 m/sec^2
i_{mc}	mean incidence angle, angle between inlet air direction and line tangent to blade mean camber line at leading edge, deg
i_{ss}	suction-surface incidence angle, angle between inlet air direction and line tangent to blade suction surface at leading edge, deg
J	mechanical equivalent of heat
M	Mach number
N	rotative speed, rpm
P	total pressure, N/cm^2
PR	total pressure ratio
ΔP	$P_{max} - P_{min}$, N/cm^2
p	static pressure, N/cm^2
Δp	$p_{max} - p_{min}$, N/cm^2
r	radius, cm
SM	stall margin
T	total temperature, K
TR	total temperature ratio
U	wheel speed, m/sec
V	air velocity, m/sec
ΔV_z	$V_{z,max} - V_{z,min}$, m/sec
ΔV_θ	$V_{\theta,max(or\ min)} - 0$ (measure of upstream induced distortion), m/sec
W	weight flow, kg/sec

Z	axial distance referenced from rotor blade hub leading edge, cm
α_c	cone angle, deg
α_s	slope of streamline, deg
β	air angle, angle between air velocity and axial direction, deg
β'_c	relative meridional air angle based on cone angle, arctan (tan β'_m cos α_c/cos α_s), deg
γ	ratio of specific heats
δ	ratio of rotor inlet total pressure to standard pressure of 10.13 N/cm^2
δ^o	deviation angle, angle between outlet air direction and tangent to blade mean camber line at trailing edge, deg
η	efficiency
θ	ratio of rotor inlet total temperature to standard temperature of 288.2 K
κ_{mc}	angle between blade mean camber line and meridional plane, deg
κ_{ss}	angle between blade suction-surface camber line at leading edge and meridional plane, deg
σ	solidity, ratio of chord to spacing
$\overline{\omega}$	total loss coefficient
$\overline{\omega}_p$	profile loss coefficient
$\overline{\omega}_s$	shock loss coefficient

Subscripts:

abs	absolute
ad	adiabatic (temperature rise)
d	distortion
id	ideal
ind	indicated
int	integrated
LE	blade leading edge
loc	local
m	meridional direction
max	maximum

min	minimum
mom	momentum rise
orif	orifice
p	polytropic
r	radial direction
ref	reference
s	stall
u	undistorted
TE	blade trailing edge
z	axial direction
θ	tangential direction
-1	instrumentation plane between distortion screen and rotor (fig. 4)
0	instrumentation plane between distortion screen and rotor (fig. 4)
1	instrumentation plane upstream of rotor (rotor inlet) (fig. 4)
2	instrumentation plane between rotor and stator (fig. 4)
3	instrumentation plane downstream of stator (fig. 4)

Superscript:

'	relative to blade

APPENDIX B

EQUATIONS

Suction-surface incidence angle:

$$i_{ss} = \left(\beta'_c\right)_{LE} - \kappa_{ss} \tag{B1}$$

Mean incidence angle:

$$i_{mc} = \left(\beta'_c\right)_{LE} - \left(\kappa_{mc}\right)_{LE} \tag{B2}$$

Deviation angle:

$$\delta^o = \left(\beta'_c\right)_{TE} - \left(\kappa_{mc}\right)_{TE} \tag{B3}$$

Diffusion factor:

$$D = 1 - \frac{V'_{TE}}{V'_{LE}} + \left|\frac{\left(rV_\theta\right)_{TE} - \left(rV_\theta\right)_{LE}}{(r_{TE} + r_{LE})\sigma(V'_{LE})}\right| \tag{B4}$$

Total loss coefficient:

$$\overline{\omega} = \frac{\left(P'_{id}\right)_{TE} - (P')_{TE}}{(P')_{LE} - (p)_{LE}} \tag{B5}$$

Profile loss coefficient:

$$\overline{\omega}_p = \overline{\omega} - \overline{\omega}_s \tag{B6}$$

Total loss parameter:

$$\frac{\overline{\omega}\cos\left(\beta'_m\right)_{TE}}{2\sigma} \tag{B7}$$

Profile loss parameter:

$$\frac{\overline{\omega}_p \cos\left(\beta'_m\right)_{TE}}{2\sigma} \tag{B8}$$

Adiabatic (temperature rise) efficiency:

$$\eta_{ad} = \frac{PR^{(\gamma-1)/\gamma} - 1}{TR - 1} \tag{B9}$$

Momentum-rise efficiency:

$$\eta_{mom} = \frac{PR^{(\gamma-1)/\gamma} - 1}{\frac{\left(UV_\theta\right)_{TE} - \left(UV_\theta\right)_{LE}}{T_{LE} g J C_p}} \tag{B10}$$

Equivalent weight flow:

$$\frac{W\sqrt{\theta}}{\delta} \tag{B11}$$

Equivalent rotative speed:

$$\frac{N}{\sqrt{\theta}} \tag{B12}$$

Equivalent weight flow per unit annulus area:

$$\frac{\left(\frac{W\sqrt{\theta}}{\delta}\right)}{A_{an}} \tag{B13}$$

Equivalent weight flow per unit frontal area:

$$\frac{\left(\frac{W\sqrt{\theta}}{\delta}\right)}{A_f} \tag{B14}$$

Head-rise coefficient:

$$\frac{gJC_pT_{LE}}{U_{tip}^2}\left[PR^{(\gamma-1)/\gamma} - 1\right] \tag{B15}$$

Flow coefficient:

$$\left(\frac{V_z}{U_{tip}}\right)_{LE} \tag{B16}$$

Stall margin:

$$SM = \left[\frac{PR_s}{PR_{ref}} \times \frac{\left(\frac{W\sqrt{\theta}}{\delta}\right)_{ref}}{\left(\frac{W\sqrt{\theta}}{\delta}\right)_s} - 1\right] \times 100 \tag{B17}$$

Loss in stall pressure ratio:

$$\Delta PR_s = 1 - \left.\frac{PR_{d,s}}{PR_{u,s}}\right|_{\frac{N}{\sqrt{\theta}}=\text{Constant}} \tag{B18}$$

APPENDIX C

DEFINITIONS AND UNITS USED IN TABLES

ABS	absolute
AERO CHORD	aerodynamic chord, cm
AREA RATIO	ratio of actual flow area to critical area (where local Mach number is 1)
BETAM	meridional air angle, deg
CONE ANGLE	angle between axial direction and conical surface representing blade element, deg
DELTA INC	difference between mean camber blade angle and suction-surface blade angle at leading edge, deg
DEV	deviation angle (defined by eq. (B3)), deg
D-FACT	diffusion factor (defined by eq. (B4))
EFF	adiabatic efficiency (defined by eq. (B9))
IN	inlet (leading edge of blade)
INCIDENCE	incidence angle (suction surface defined by eq. (B1) and mean defined by eq. (B2))
KIC	angle between blade mean camber line at leading edge and meridional plane, deg
KOC	angle between blade mean camber line at trailing edge and meridional plane, deg
KTC	angle between blade mean camber line at transition point and meridional plane, deg
LOSS COEFF	loss coefficient (total defined by eq. (B5) and profile defined by eq. (B6))
LOSS PARAM	loss parameter (total defined by eq. (B7) and profile defined by eq. (B8))
MERID	meridional
MERID VEL R	meridional velocity ratio
OUT	outlet (trailing edge of blade)
PERCENT SPAN	percent of blade span from tip at rotor outlet

PHISS	suction-surface camber ahead of assumed shock location, deg
PRESS	pressure, N/cm^2
PROF	profile
RADII	radius, cm
REL	relative to blade
RI	inlet radius (leading edge of blade), cm
RO	outlet radius (trailing edge of blade), cm
RP	radial position
RPM	equivalent rotative speed, rpm
SETTING ANGLE	angle between aerodynamic chord and meridional plane, deg
SOLIDITY	ratio of aerodynamic chord to blade spacing
SPEED	speed, m/sec
SS	suction surface
STREAMLINE SLOPE	slope of streamline, deg
TANG	tangential
TEMP	temperature, K
TI	thickness of blade at leading edge, cm
TM	thickness of blade at maximum thickness, cm
TO	thickness of blade at trailing edge, cm
TOT	total
TOTAL CAMBER	difference between inlet and outlet blade mean camber lines, deg
VEL	velocity, m/sec
WT FLOW	equivalent weight flow, kg/sec
X FACTOR	ratio of suction-surface camber ahead of assumed shock location of a multiple-circular-arc blade section to that of a double-circular-arc blade section
ZIC	axial distance to blade leading edge from inlet, cm
ZMC	axial distance to blade maximum thickness point from inlet, cm
ZOC	axial distance to blade trailing edge from inlet, cm
ZTC	axial distance to transition point from inlet, cm

REFERENCES

1. Kovich, George; Moore, Royce D.; and Urasek, Donald C.: Performance of Transonic Fan Stage with Weight Flow per Unit Annulus Area of 198 Kilograms per Second per Square Meter (40.6 (lb/sec)/ft^2). NASA TM X-2905, 1973.

2. Urasek, Donald C.; and Janetzke, David C.: Performance of Tandem-Bladed Transonic Compressor Rotor with Tip Speed of 1375 Feet Per Second. NASA TM X-2484, 1972.

3. Glawe, George E.; Krause, Lloyd N.; and Dudzinski, Thomas J.: A Small Combination Sensing Probe for Measurement of Temperature, Pressure, and Flow Direction. NASA TN D-4816, 1968.

4. Callahan, G. M.; and Stenning, A. H.: Attenuation of Inlet Flow Distortion Upstream of Axial Flow Compressors. AIAA Paper 69-485, June 1969.

5. Katz, Robert: Performance of Axial Compressors with Asymmetric Inlet Flows. California Inst. of Tech. (AFOSR-TR-58-89; AD-162112), 1958.

6. Greitzer, E. M.: Upstream Attenuation and Quasi-Steady Rotor Lift Fluctuations in Asymmetric Flows in Axial Compressors. ASME Paper 73-GT-30, Apr. 1973.

7. Adamczyk, John J.; and Carta, Franklin O.: Unsteady Fluid Dynamic Response of an Axial Flow Compressor Stage with Distorted Inflow. SQUID-TR-UARL-2-PU; UARL-M91103-7, Purdue Univ. (AD-766084), 1973.

8. Dicus, John H.: FORTRAN Program to Generate Engine Inlet Flow Contour Maps and Distortion Parameters. NASA TM X-2967, 1974.

9. Dunham, J.: Non-Axisymmetric Flows in Axial Compressors. Mech. Eng. Sci. Monograph No. 3, Inst. Mech. Eng. (Great Britain), 1965.

10. Carta, Franklin O.: Unsteady Normal Force on an Airfoil in a Periodically Stalled Inlet Flow. J. Aircraft, vol. 4, no. 5, Sept.-Oct. 1967, pp. 416-421.

11. Reid, C.: The Response of Axial Flow Compressors to Intake Flow Distortion. ASME Paper 69-GT-29, Mar. 1969.

TABLE I. - DESIGN OVERALL PARAMETERS

FOR STAGE 11-4

ROTOR TOTAL PRESSURE RATIO	1.601
STAGE TOTAL PRESSURE RATIO	1.574
ROTOR TOTAL TEMPERATURE RATIO	1.162
STAGE TOTAL TEMPERATURE RATIO	1.162
ROTOR ADIABATIC EFFICIENCY	0.809
STAGE ADIABATIC EFFICIENCY	0.855
ROTOR POLYTROPIC EFFICIENCY	0.896
STAGE POLYTROPIC EFFICIENCY	0.864
ROTOR HEAD RISE COEFFICIENT	0.231
STAGE HEAD RISE COEFFICIENT	0.222
FLOW COEFFICIENT	0.457
WT FLOW PER UNIT FRONTAL AREA	147.822
WT FLOW PER UNIT ANNULUS AREA	198.166
WT FLOW	29.484
RPM	16100.000
TIP SPEED	424.815

TABLE II. - DESIGN BLADE-ELEMENT PARAMETERS FOR ROTOR 11

	RADII		ABS BETAM		REL BETAM		TOTAL TEMP		TOTAL PRESS	
RP	IN	OUT	IN	OUT	IN	OUT	IN	RATIO	IN	RATIO
TIP	25.197	24.816	0.	43.1	67.1	62.6	288.2	1.198	10.13	1.601
1	24.628	24.280	-0.	41.3	66.1	61.7	288.2	1.186	10.13	1.601
2	24.060	23.744	0.	40.0	65.1	60.7	288.2	1.177	10.13	1.601
3	21.741	21.600	0.	39.3	61.5	56.0	288.2	1.163	10.13	1.601
4	19.980	19.992	0.	40.0	59.1	51.5	288.2	1.157	10.13	1.601
5	19.658	19.724	0.	40.2	58.7	50.6	288.2	1.157	10.13	1.601
6	19.356	19.456	0.	40.4	58.2	49.7	288.2	1.156	10.13	1.601
7	19.052	19.188	0.	40.7	57.8	48.7	288.2	1.156	10.13	1.601
8	18.747	18.920	0.	40.9	57.4	47.6	288.2	1.155	10.13	1.601
9	16.871	17.313	0.	42.5	54.9	40.4	288.2	1.153	10.13	1.601
10	14.202	15.169	0.	45.8	51.1	26.0	288.2	1.153	10.13	1.601
11	13.492	14.635	0.	47.1	50.0	21.0	288.2	1.155	10.13	1.601
HUB	12.700	14.097	0.	48.4	48.7	15.4	288.2	1.157	10.13	1.601

	ABS VEL		REL VEL		MERID VEL		TANG VEL		WHEEL SPEED	
RP	IN	OUT	IN	OUT	IN	OUT	IN	OUT	IN	OUT
TIP	179.2	199.9	461.1	317.2	179.2	145.9	0.	136.7	424.8	418.4
1	184.1	199.1	454.2	315.8	184.1	149.7	-0.	131.3	415.2	409.4
2	188.4	199.2	447.3	312.2	188.4	152.7	0.	127.9	405.7	400.3
3	198.8	204.3	417.0	285.2	198.8	158.2	0.	129.3	366.5	364.2
4	201.7	210.0	392.3	258.2	201.7	160.8	0.	135.1	336.5	337.1
5	201.9	211.2	388.1	253.9	201.9	161.2	0.	136.4	331.4	332.6
6	202.0	212.4	383.8	249.7	202.0	161.6	0.	137.8	326.3	328.0
7	202.0	213.6	379.4	245.4	202.0	162.0	0.	139.2	321.2	323.5
8	201.9	215.0	375.0	241.2	201.9	162.5	0.	140.8	316.1	319.0
9	200.0	224.2	347.7	216.9	200.0	165.3	0.	151.5	284.4	291.9
10	192.9	241.9	307.5	187.6	192.9	168.6	0.	173.5	259.4	255.7
11	190.6	248.1	296.8	181.1	190.6	169.0	0.	181.7	227.5	246.7
HUB	188.0	255.2	284.9	175.6	188.0	169.3	0.	191.0	214.1	257.7

	ABS MACH NO		REL MACH NO		MERID MACH NO		STREAMLINE SLOPE		MERID PEAK SS	
RP	IN	OUT	IN	OUT	IN	OUT	IN	OUT	VEL R	MACH NO
TIP	0.542	0.553	1.394	0.878	0.542	0.404	-5.69	-8.84	0.814	1.562
1	0.553	0.554	1.376	0.878	0.558	0.416	-5.12	-7.72	0.813	1.549
2	0.571	0.556	1.357	0.872	0.571	0.426	-4.46	-6.60	0.810	1.539
3	0.605	0.575	1.270	0.797	0.605	0.445	-0.98	-2.24	0.798	1.519
4	0.615	0.594	1.196	0.730	0.615	0.455	2.14	0.87	0.797	1.509
5	0.615	0.597	1.183	0.718	0.615	0.456	2.70	1.39	0.799	1.508
6	0.616	0.601	1.170	0.707	0.616	0.457	3.28	1.92	0.800	1.507
7	0.616	0.605	1.157	0.695	0.616	0.459	3.86	2.44	0.802	1.506
8	0.615	0.609	1.143	0.683	0.615	0.460	4.46	2.97	0.805	1.506
9	0.609	0.633	1.059	0.617	0.609	0.470	8.45	6.33	0.826	1.501
10	0.583	0.695	0.954	0.537	0.586	0.483	15.38	11.44	0.874	1.467
11	0.579	0.712	0.901	0.520	0.579	0.485	17.58	12.87	0.887	1.431
HUB	0.570	0.734	0.864	0.505	0.570	0.487	20.23	14.35	0.901	1.379

	PERCENT	INCIDENCE		DEV	D-FACT	EFF	LOSS COEFF		LOSS PARAM	
RP	SPAN	MEAN	SS				TOT	PROF	TOT	PROF
TIP	0.	2.5	-0.0	4.8	0.425	0.728	0.212	0.119	0.038	0.021
1	5.00	2.8	-0.0	4.4	0.413	0.774	0.171	0.085	0.031	0.015
2	10.00	3.0	0.0	4.0	0.407	0.813	0.140	0.058	0.025	0.010
3	30.00	4.1	-0.0	2.9	0.424	0.884	0.088	0.024	0.017	0.004
4	45.00	4.9	0.0	2.7	0.449	0.914	0.069	0.016	0.013	0.003
5	47.50	5.1	0.0	2.7	0.453	0.918	0.067	0.016	0.013	0.003
6	50.00	5.2	0.0	2.7	0.458	0.921	0.065	0.016	0.013	0.003
7	52.50	5.4	0.0	2.8	0.462	0.924	0.063	0.016	0.012	0.003
8	55.00	5.5	-0.0	2.8	0.467	0.927	0.062	0.016	0.012	0.003
9	70.00	6.3	0.0	3.5	0.492	0.942	0.054	0.020	0.011	0.004
10	90.00	7.3	0.0	5.6	0.519	0.938	0.069	0.052	0.014	0.010
11	95.00	7.5	0.0	6.3	0.524	0.929	0.084	0.073	0.017	0.014
HUB	100.00	7.6	-0.1	7.1	0.523	0.917	0.107	0.102	0.020	0.019

TABLE III. - DESIGN BLADE-ELEMENT PARAMETERS FOR STATOR 4

	RADII		ABS BETAM		REL BETAM		TOTAL TEMP		TOTAL PRESS	
RP	IN	OUT	IN	OUT	IN	OUT	IN	RATIO	IN	RATIO
TIP	24.394	24.384	38.3	0.	38.3	0.	345.2	1.000	16.22	0.983
1	23.919	23.908	36.7	-0.	36.7	-0.	341.7	1.000	16.22	0.981
2	23.453	23.459	35.7	0.	35.7	0.	339.1	1.000	16.22	0.982
3	21.557	21.636	35.5	0.	35.5	0.	335.0	1.000	16.22	0.989
4	20.113	20.265	36.3	0.	36.3	0.	333.5	1.000	16.22	0.988
5	19.872	20.038	36.5	0.	36.5	0.	333.3	1.000	16.22	0.987
6	19.630	19.810	36.7	0.	36.7	0.	333.2	1.000	16.22	0.987
7	19.388	19.582	36.9	0.	36.9	0.	333.0	1.000	16.22	0.987
8	19.146	19.355	37.2	0.	37.2	0.	332.9	1.000	16.22	0.986
9	17.692	18.004	38.6	0.	38.6	0.	332.2	1.000	16.22	0.984
10	15.755	16.239	41.6	0.	41.6	0.	332.3	1.000	16.22	0.974
11	15.273	15.805	42.8	0.	42.8	0.	332.8	1.000	16.22	0.966
HUB	14.643	15.240	44.4	-0.	44.4	-0.	333.5	1.000	16.22	0.953

	ABS VEL		REL VEL		MERID VEL		TANG VEL		WHEEL SPEED	
RP	IN	OUT	IN	OUT	IN	OUT	IN	OUT	IN	OUT
TIP	224.5	177.1	224.5	177.1	176.1	177.1	139.3	0.	0.	0.
1	222.9	176.2	222.9	176.2	178.7	176.2	135.3	-0.	0.	0.
2	222.1	176.0	222.1	176.0	180.5	176.0	129.5	0.	0.	0.
3	223.4	179.2	223.4	179.2	181.9	179.2	129.6	0.	0.	0.
4	226.7	179.9	226.7	179.9	182.6	179.9	134.3	0.	0.	0.
5	227.5	180.0	227.5	180.0	182.8	180.0	135.4	0.	0.	0.
6	228.3	180.2	228.3	180.2	183.0	180.2	136.5	0.	0.	0.
7	229.3	180.4	229.3	180.4	183.2	180.4	137.8	0.	0.	0.
8	230.2	180.6	230.2	180.6	183.5	180.6	139.1	0.	0.	0.
9	237.4	182.3	237.4	182.3	185.4	182.3	148.2	0.	0.	0.
10	251.3	182.5	251.3	182.5	187.8	182.5	167.0	0.	0.	0.
11	255.2	181.4	255.2	181.4	188.1	181.4	174.0	0.	0.	0.
HUB	263.6	179.3	263.6	179.3	188.3	179.3	184.4	-0.	0.	0.

	ABS MACH NO		REL MACH NO		MERID MACH NO		STREAMLINE SLOPE		MERID PEAK SS	
RP	IN	OUT	IN	OUT	IN	OUT	IN	OUT	VEL R	MACH NO
TIP	0.626	0.487	0.626	0.487	0.491	0.487	-1.16	-0.06	1.006	0.905
1	0.625	0.487	0.625	0.487	0.501	0.487	-0.70	0.11	0.996	0.894
2	0.625	0.488	0.625	0.488	0.508	0.488	-0.29	0.26	0.975	0.870
3	0.633	0.501	0.633	0.501	0.515	0.501	1.25	0.91	0.993	0.885
4	0.644	0.504	0.644	0.504	0.519	0.504	2.59	1.54	0.995	0.878
5	0.647	0.504	0.647	0.504	0.520	0.504	2.84	1.65	0.995	0.882
6	0.650	0.505	0.650	0.505	0.521	0.505	3.09	1.77	0.995	0.886
7	0.653	0.506	0.653	0.506	0.522	0.506	3.36	1.89	0.994	0.890
8	0.656	0.506	0.656	0.506	0.523	0.506	3.63	2.01	0.994	0.894
9	0.679	0.512	0.679	0.512	0.530	0.512	5.48	2.81	0.985	0.925
10	0.725	0.512	0.725	0.512	0.540	0.512	8.68	4.02	0.972	0.992
11	0.738	0.509	0.738	0.509	0.542	0.509	9.65	4.30	0.964	1.017
HUB	0.761	0.502	0.761	0.502	0.543	0.502	10.99	4.64	0.952	1.055

	PERCENT	INCIDENCE		DEV	D-FACT	EFF	LOSS COEFF		LOSS PARAM	
RP	SPAN	MEAN	SS				TOT	PROF	TOT	PROF
TIP	0.	6.4	-0.0	10.7	0.455	0.	0.080	0.080	0.032	0.032
1	5.00	6.4	0.0	9.7	0.441	0.	0.082	0.082	0.031	0.031
2	10.00	6.4	-0.0	9.0	0.428	0.	0.079	0.079	0.030	0.030
3	30.00	6.4	0.0	8.2	0.399	0.	0.047	0.047	0.016	0.016
4	45.00	6.4	0.0	8.0	0.399	0.	0.051	0.051	0.017	0.017
5	47.50	6.4	0.0	8.0	0.399	0.	0.052	0.052	0.017	0.017
6	50.00	6.4	0.0	8.0	0.400	0.	0.053	0.053	0.017	0.017
7	52.50	6.4	0.0	8.0	0.401	0.	0.054	0.054	0.017	0.017
8	55.00	6.4	0.0	8.0	0.402	0.	0.055	0.055	0.017	0.017
9	70.00	6.4	0.0	7.9	0.410	0.	0.060	0.060	0.017	0.017
10	90.00	6.3	0.0	8.1	0.442	0.	0.088	0.088	0.025	0.025
11	95.00	6.3	0.0	8.3	0.458	0.	0.111	0.111	0.027	0.027
HUB	100.00	6.2	-0.0	8.5	0.483	0.	0.146	0.146	0.035	0.035

TABLE IV. - BLADE GEOMETRY FOR ROTOR 11

RP	PERCENT SPAN	RADII RI	RADII RO	BLADE ANGLES KIC	BLADE ANGLES KTC	BLADE ANGLES KOC	DELTA INC	CONE ANGLE
TIP	0.	25.197	24.816	64.37	62.97	57.71	2.53	-10.431
1	5.	24.628	24.280	63.11	61.83	57.26	2.78	-9.182
2	10.	24.060	23.744	61.90	60.58	56.65	3.04	-8.035
3	30.	21.741	21.600	57.36	54.88	53.15	4.13	-3.095
4	45.	19.980	19.992	54.13	50.29	48.79	4.95	0.651
5	48.	19.658	19.724	53.59	49.49	47.87	5.09	1.291
6	50.	19.336	19.456	53.05	48.68	46.91	5.22	1.935
7	53.	19.052	19.188	52.51	47.86	45.89	5.36	2.581
8	55.	18.747	18.920	51.97	47.02	44.82	5.49	3.232
9	70.	16.871	17.313	48.65	42.07	36.74	6.30	7.403
10	90.	14.202	15.169	44.05	34.00	20.19	7.28	13.919
11	95.	13.492	14.633	42.82	31.93	14.48	7.49	15.774
HUB	100.	12.700	14.097	41.44	29.85	8.02	7.69	18.485

RP	BLADE THICKNESSES TI	BLADE THICKNESSES TM	BLADE THICKNESSES TO	AXIAL DIMENSIONS ZIC	AXIAL DIMENSIONS ZMC	AXIAL DIMENSIONS ZTC	AXIAL DIMENSIONS ZOC
TIP	0.051	0.152	0.051	1.046	2.039	2.444	3.116
1	0.051	0.162	0.051	1.002	2.040	2.415	3.156
2	0.051	0.172	0.051	0.955	2.040	2.381	3.198
3	0.051	0.215	0.051	0.761	2.027	2.191	3.363
4	0.051	0.248	0.051	0.621	2.021	2.003	3.502
5	0.051	0.254	0.051	0.598	2.019	1.967	3.527
6	0.051	0.260	0.051	0.574	2.018	1.930	3.553
7	0.051	0.265	0.051	0.550	2.017	1.892	3.579
8	0.051	0.271	0.051	0.526	2.016	1.852	3.606
9	0.051	0.306	0.051	0.377	2.003	1.588	3.774
10	0.051	0.356	0.051	0.147	1.989	1.143	4.050
11	0.051	0.370	0.051	0.079	1.983	1.013	4.116
HUB	0.051	0.385	0.051	0.000	1.972	0.861	4.179

RP	AERO CHORD	SETTING ANGLE	TOTAL CAMBER	SOLIDITY	X FACTOR	PHISS	AREA RATIO
TIP	4.634	62.67	6.66	1.298	0.704	4.94	1.040
1	4.628	61.53	5.85	1.325	0.747	5.04	1.040
2	4.625	60.33	5.25	1.355	0.799	5.30	1.040
3	4.616	55.20	4.21	1.492	1.011	7.12	1.039
4	4.614	50.86	5.34	1.618	1.110	8.71	1.039
5	4.615	50.06	5.72	1.641	1.122	8.99	1.039
6	4.615	49.24	6.15	1.665	1.132	9.27	1.039
7	4.616	48.39	6.62	1.691	1.142	9.55	1.039
8	4.618	47.52	7.16	1.717	1.151	9.85	1.039
9	4.636	41.66	11.91	1.899	1.165	11.30	1.039
10	4.716	30.45	23.86	2.249	1.242	13.97	1.040
11	4.753	26.85	28.34	2.367	1.256	14.51	1.040
HUB	4.830	22.79	33.41	2.525	1.251	14.85	1.041

TABLE V. - BLADE GEOMETRY FOR STATOR 4

RP	PERCENT SPAN	RADII RI	RADII RO	BLADE ANGLES KIC	BLADE ANGLES KTC	BLADE ANGLES KOC	DELTA INC	CONE ANGLE
TIP	0.	24.384	24.384	51.97	26.38	-10.67	6.38	-0.151
1	5.	23.919	23.908	50.32	25.41	-9.67	6.40	-0.160
2	10.	23.455	23.459	29.26	24.80	-9.00	6.41	0.092
3	30.	21.557	21.603	29.04	24.96	-8.21	6.41	1.158
4	45.	20.115	20.265	29.94	25.83	-8.02	6.40	2.248
5	48.	19.872	20.033	30.14	26.01	-8.01	6.39	2.450
6	50.	19.630	19.810	30.35	26.20	-7.99	6.39	2.659
7	53.	19.388	19.582	30.57	26.40	-7.98	6.39	2.874
8	55.	19.146	19.355	30.81	26.61	-7.97	6.38	3.096
9	70.	17.692	18.004	32.31	27.97	-7.93	6.36	4.621
10	90.	15.765	16.259	35.44	30.68	-8.11	6.30	7.232
11	95.	15.275	15.805	36.61	31.66	-8.25	6.28	7.960
HUB	100.	14.645	15.240	38.35	33.10	-8.48	6.25	8.954

RP	BLADE THICKNESSES TI	BLADE THICKNESSES TM	BLADE THICKNESSES TO	AXIAL DIMENSIONS ZIC	AXIAL DIMENSIONS ZMC	AXIAL DIMENSIONS ZTC	AXIAL DIMENSIONS ZOC
TIP	0.051	0.279	0.051	7.085	8.897	8.415	10.955
1	0.051	0.279	0.051	7.068	8.901	8.355	10.955
2	0.051	0.279	0.051	7.066	8.902	8.273	10.955
3	0.051	0.279	0.051	7.047	8.898	8.167	10.928
4	0.051	0.279	0.051	7.052	8.896	8.121	10.926
5	0.051	0.279	0.051	7.053	8.895	8.115	10.925
6	0.051	0.279	0.051	7.055	8.894	8.108	10.925
7	0.051	0.279	0.051	7.056	8.894	8.102	10.924
8	0.051	0.279	0.051	7.057	8.893	8.096	10.924
9	0.051	0.279	0.051	7.066	8.886	8.057	10.919
10	0.051	0.279	0.051	7.095	8.880	8.025	10.916
11	0.051	0.279	0.051	7.106	8.876	8.022	10.914
HUB	0.051	0.279	0.051	7.123	8.871	8.020	10.911

RP	AERO CHORD	SETTING ANGLE	TOTAL CAMBER	SOLIDITY	X FACTOR	PHISS	AREA RATIO
TIP	4.053	15.81	42.63	1.270	0.600	10.33	1.194
1	4.055	14.90	40.00	1.295	0.600	9.41	1.184
2	4.055	14.35	38.27	1.320	0.600	8.77	1.176
3	4.054	14.15	37.26	1.434	0.600	8.05	1.157
4	4.056	14.54	37.96	1.535	0.600	7.92	1.141
5	4.056	14.64	38.14	1.553	0.600	7.92	1.138
6	4.057	14.74	38.34	1.572	0.600	7.91	1.135
7	4.058	14.84	38.55	1.591	0.600	7.91	1.132
8	4.058	14.96	38.78	1.611	0.600	7.91	1.129
9	4.065	15.67	40.24	1.740	0.600	7.92	1.106
10	4.083	17.19	43.55	1.950	0.600	8.18	1.077
11	4.088	17.76	44.86	2.010	0.600	8.35	1.070
HUB	4.098	18.62	46.83	2.095	0.600	8.62	1.061

TABLE VI. - BLADE-ELEMENT PARAMETERS AT NEAR-STALL CONDITION

FOR DESIGN SPEED - BACKUP SCREEN TEST

Parameter	Rotor			Stator		
	Percentage of span from tip					
	10 (tip)	50 (damper)	90 (hub)	10 (tip)	50 (damper)	90 (hub)
Suction-surface incidence angle, i_{ss}, deg	3.7	3.2	2.9	8.8	7.7	2.4
Deviation angle, δ^o, deg	0.2	2.3	7.9	14.4	8.8	10.0
Total loss coefficient, $\overline{\omega}$	0.220	0.165	0.142	0.153	0.128	0.108
Diffusion factor, D	0.515	0.534	0.539	0.459	0.505	0.499
Meridional velocity ratio, $V_{m,out}/V_{m,in}$	0.95	0.84	0.89	1.09	0.99	0.93

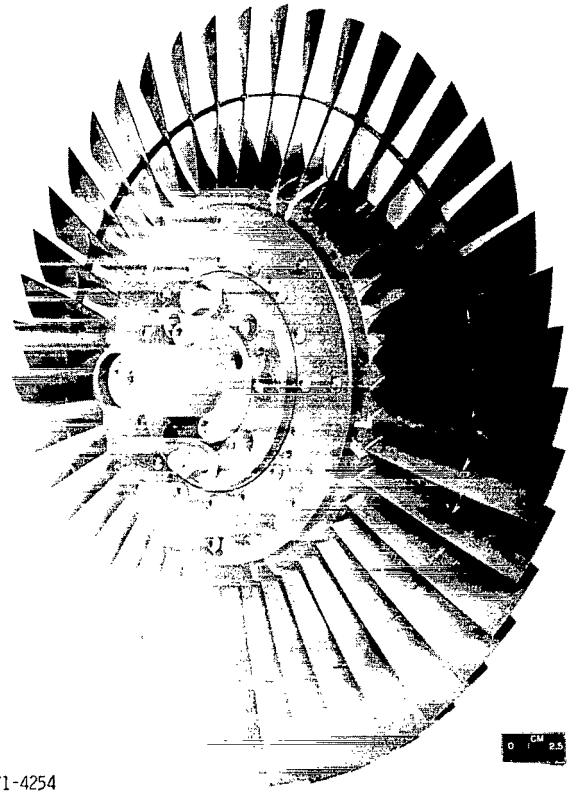

C-71-4254

Figure 1. - Rotor 11.

Figure 2. - Stator 4.

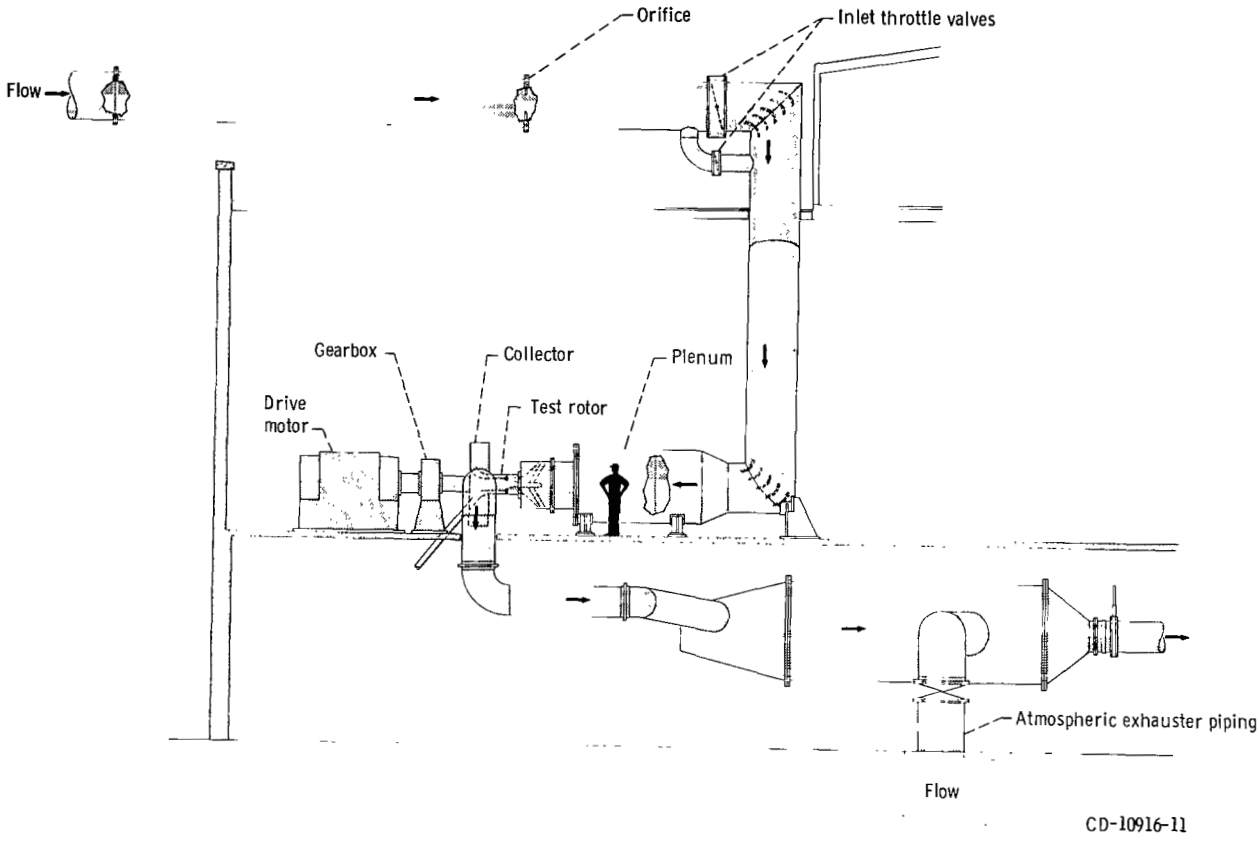

Figure 3. - Test facility.

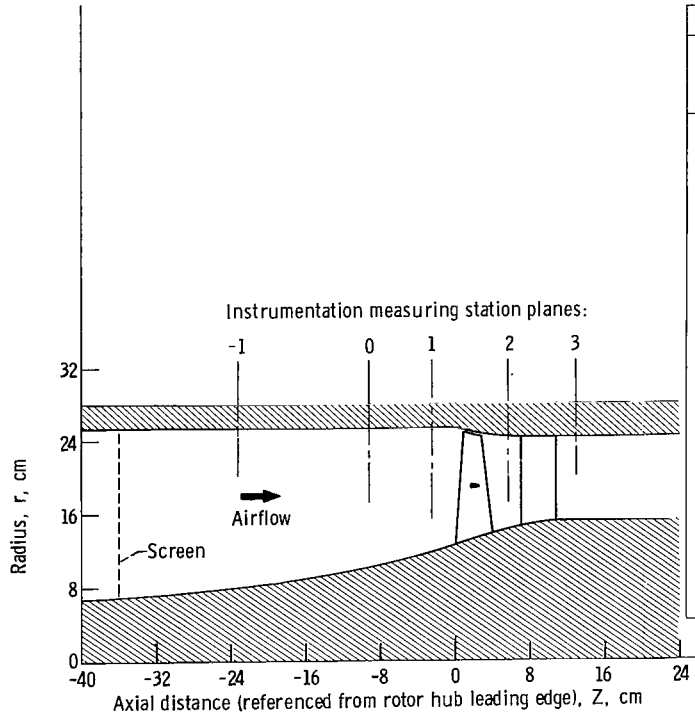

Flow path coordinates		
Axial distance, Z, cm	Radius, r, cm	
	Inner	Outer
-35.560	7.302	
-30.480	7.302	
-25.400	7.493	
[a]-22.860	7.874	
-20.320	8.255	
-15.240	9.144	
-12.700	9.589	
[a]-10.480	10.050	
-10.160	10.096	
-7.620	10.515	
-5.080	11.049	
[a]-2.540	11.747	
0	12.668	25.336
4.064	13.970	24.638
[a]5.080	14.336	24.460
7.620	14.732	24.384
10.973	15.240	
[a]12.700		
15.240		
17.780		
20.320		

[a]Measuring station.

Figure 4. - Flow path schematic for stage 11-4, showing axial location of instrumentation.

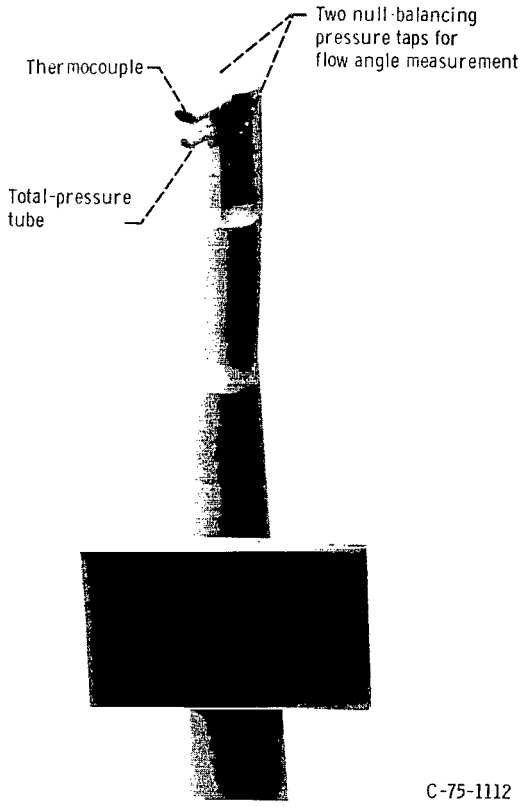

Figure 5. - Combination total pressure, total temperature, and flow angle probe (double barrel).

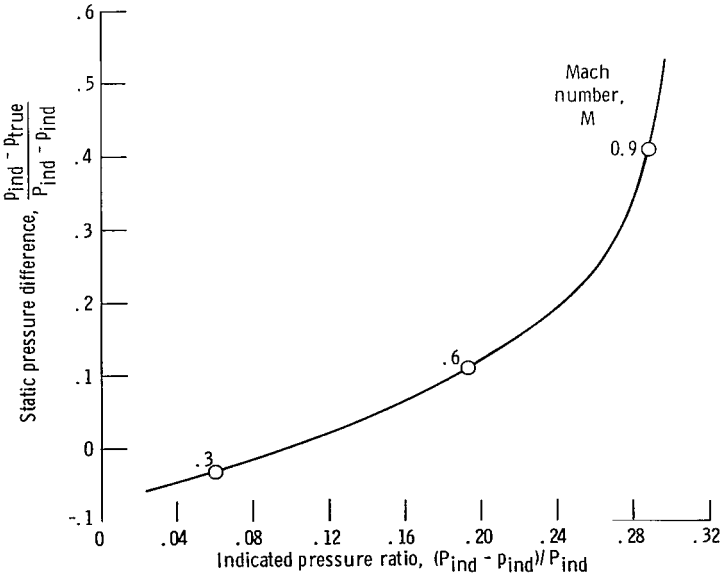

Figure 6. - Variation in static pressure difference with probe measurements for alined flow.

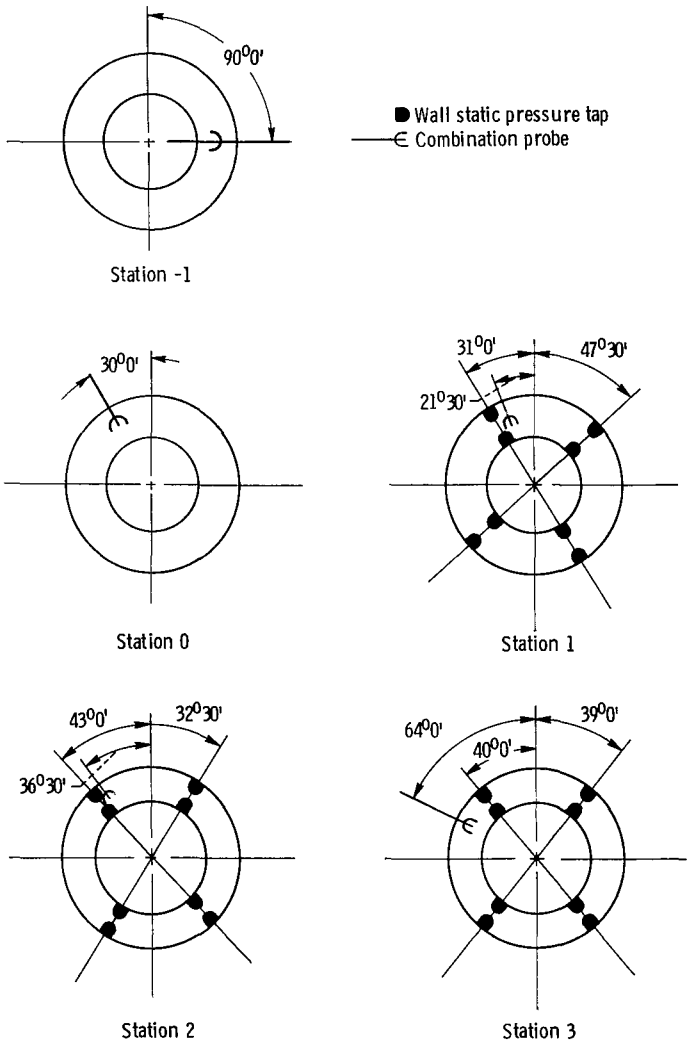

Figure 7. - Circumferential locations of measurements (looking downstream; clockwise rotation).

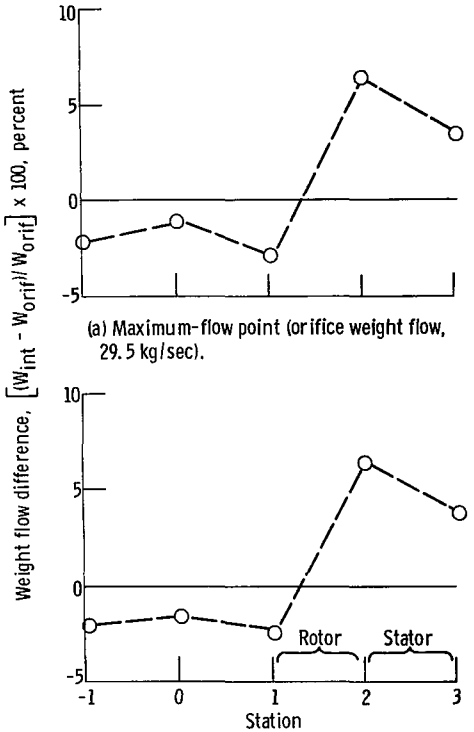

(a) Maximum-flow point (orifice weight flow, 29.5 kg/sec).

(b) Near-stall point (orifice weight flow, 27.6 kg/sec.

Figure 8. - Difference between orifice and integrated weight flows at each axial station. 90° Circumferential distortion; 100 percent of design speed.

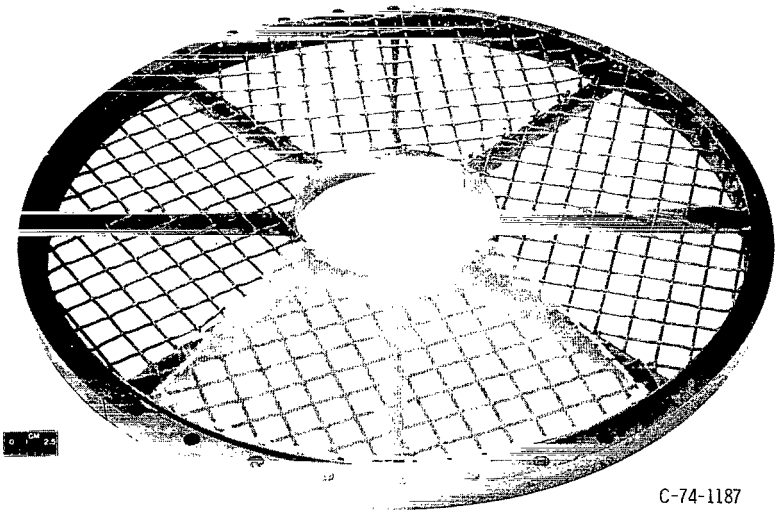

Figure 9. - Distortion screen and backup screen assembly.

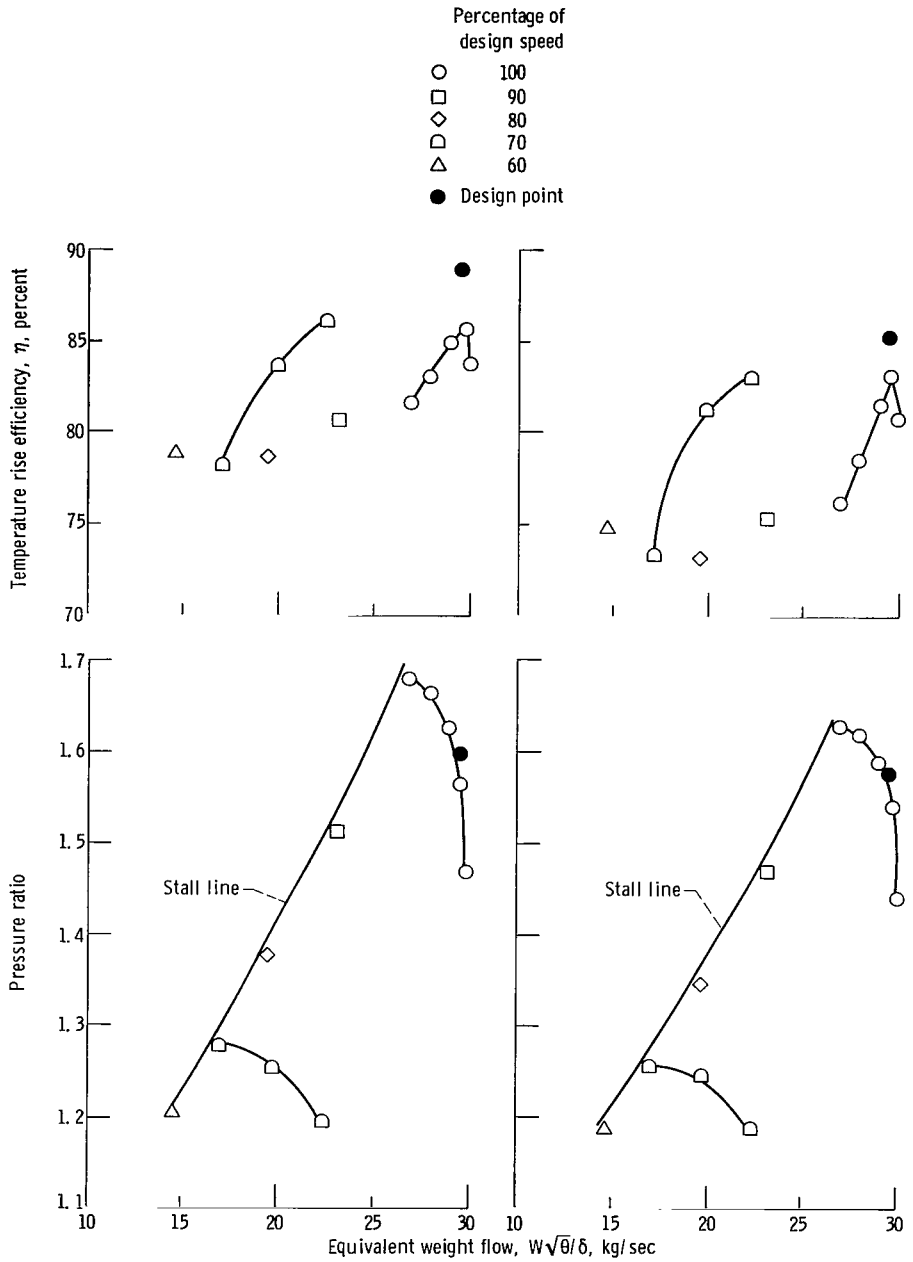

(a) Rotor 11. (b) Stage 11-4.

Figure 10. - Overall performance with backup screen in place (undistorted inlet flow).

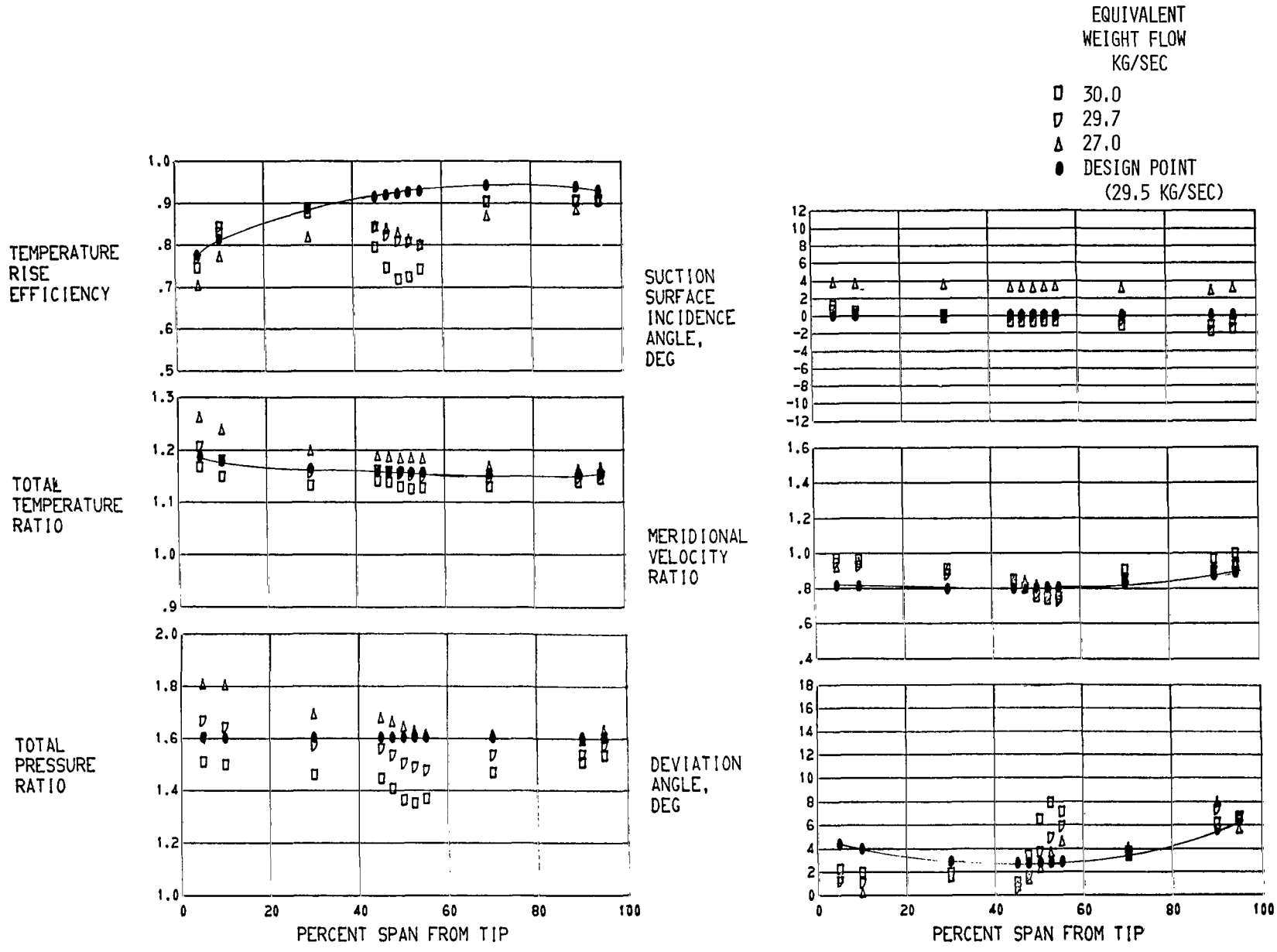
EQUIVALENT
WEIGHT FLOW
KG/SEC
30.0
29.7
27.0
DESIGN POINT
(29.5 KG/SEC)
TEMPERATURE
RISE
EFFICIENCY
TOTAL
TEMPERATURE
RATIO
TOTAL
PRESSURE
RATIO
SUCTION
SURFACE
INCIDENCE
ANGLE,
DEG
MERIDIONAL
VELOCITY
RATIO
DEVIATION
ANGLE,
DEG
PERCENT SPAN FROM TIP
PERCENT SPAN FROM TIP

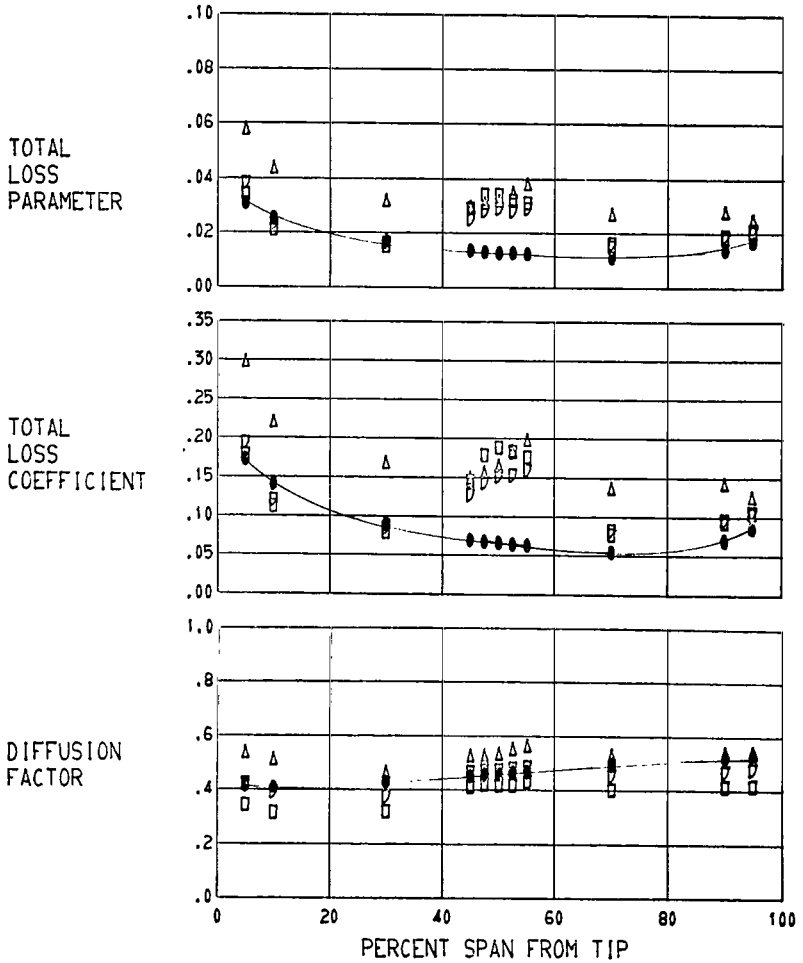

FIGURE 11. - RADIAL DISTRIBUTION OF PERFORMANCE PARAMETERS FOR ROTOR 11. BACKUP SCREEN IN PLACE; 100 PERCENT OF DESIGN SPEED.

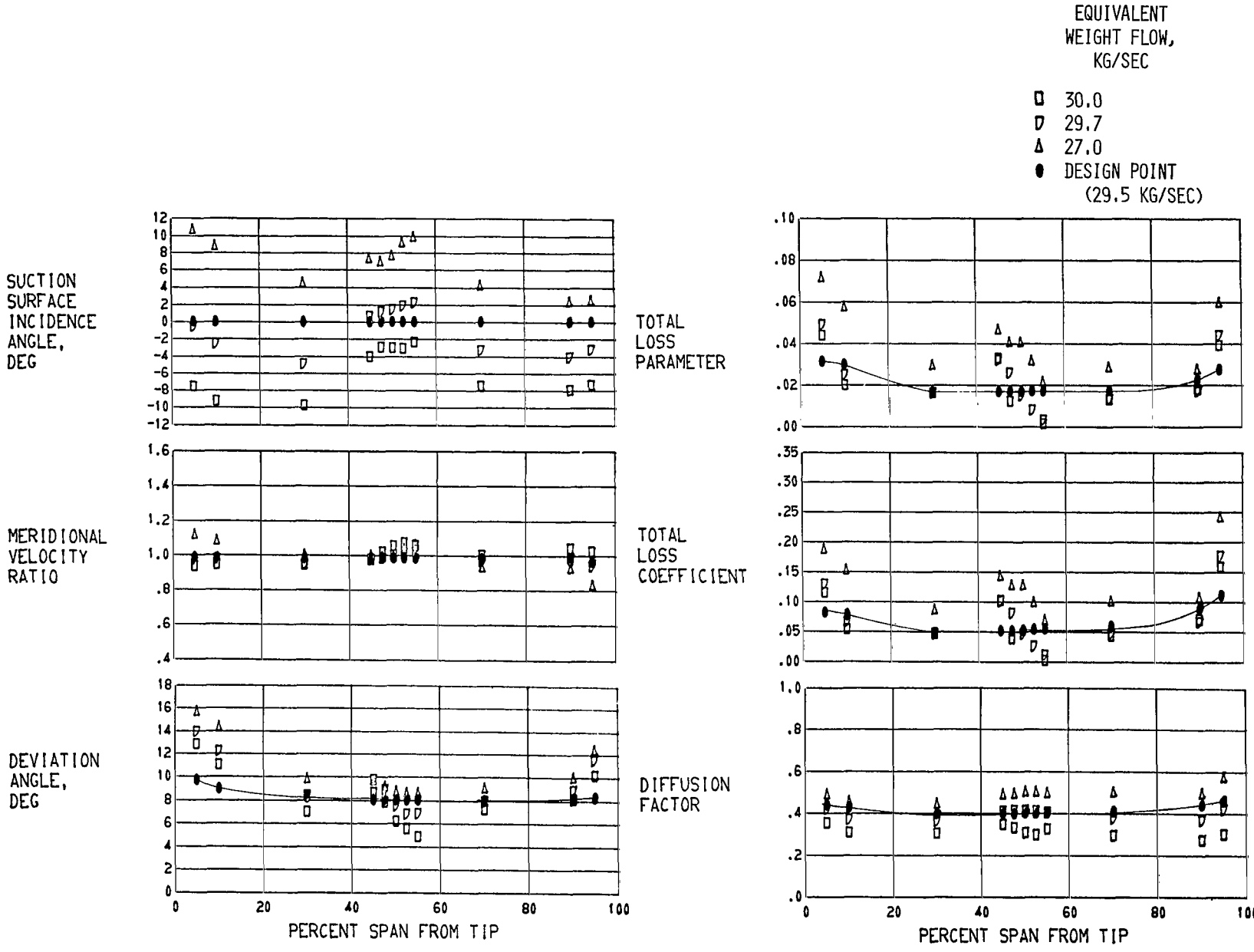

FIGURE 12. - RADIAL DISTRIBUTION OF PERFORMANCE PARAMETERS FOR STATOR 4. BACKUP SCREEN IN PLACE; 100 PERCENT OF DESIGN SPEED.

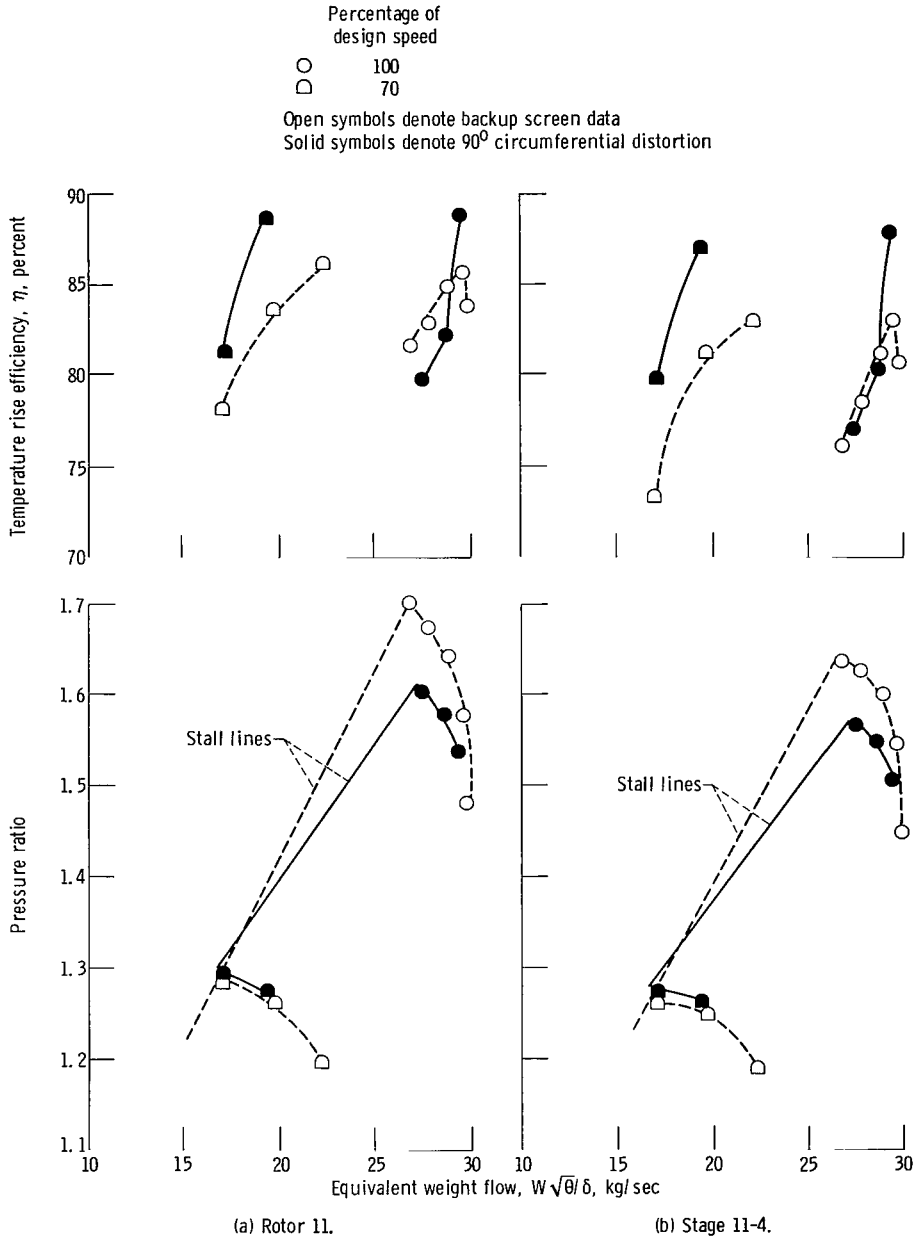

(a) Rotor 11. (b) Stage 11-4.

Figure 13. - Overall performance with distorted and undistorted inlet flow.

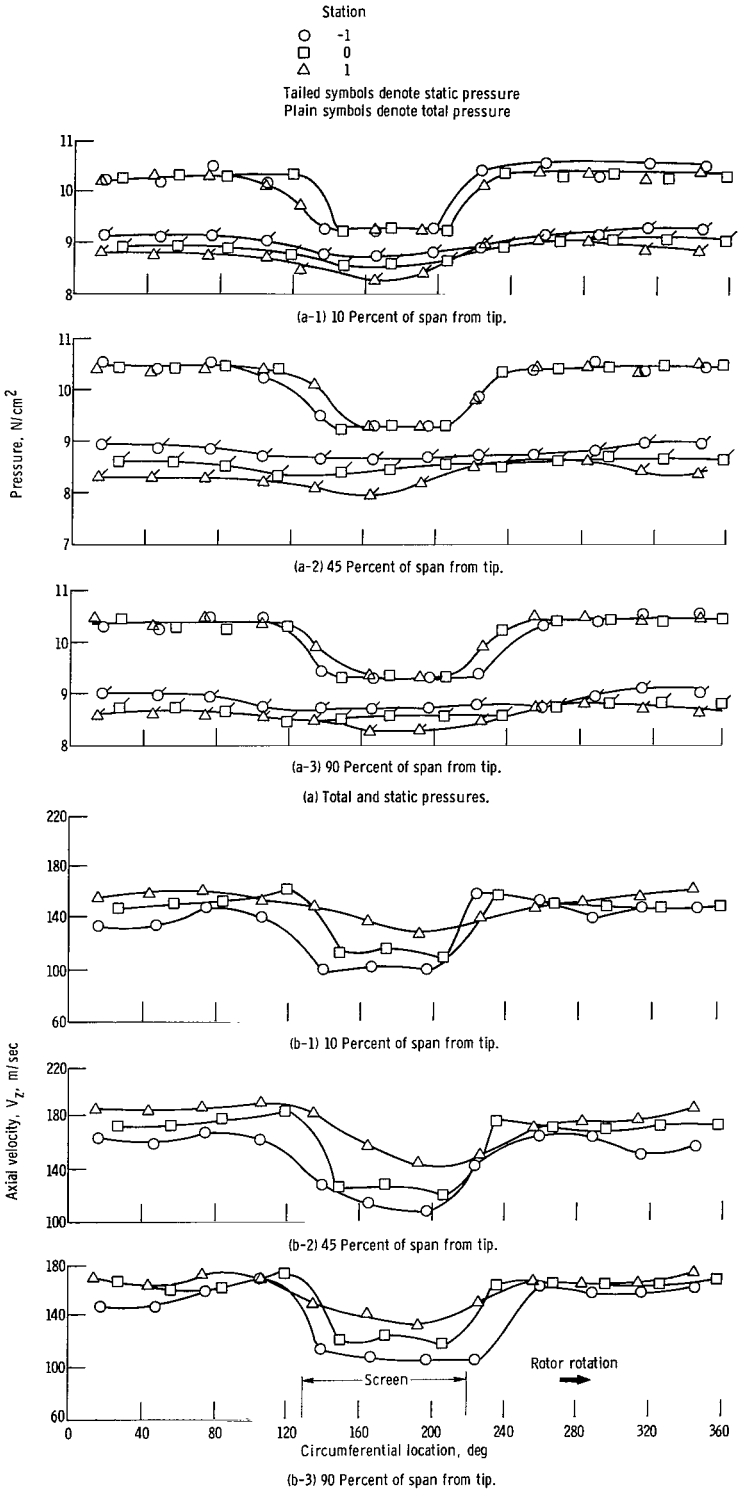

Figure 14. - Circumferential distribution of flow parameters between screen and rotor at near-stall conditions. 100 Percent of design speed.

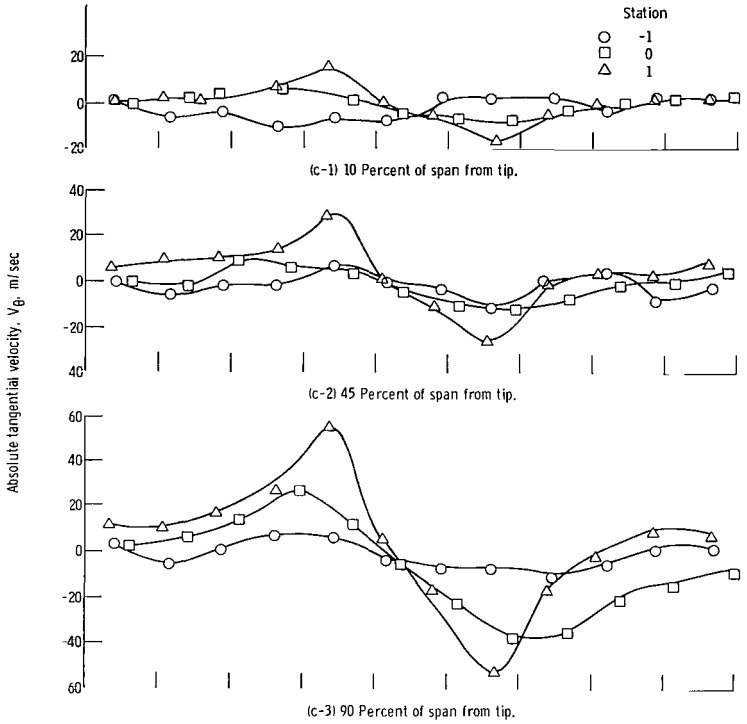

(c) Absolute tangential velocity.

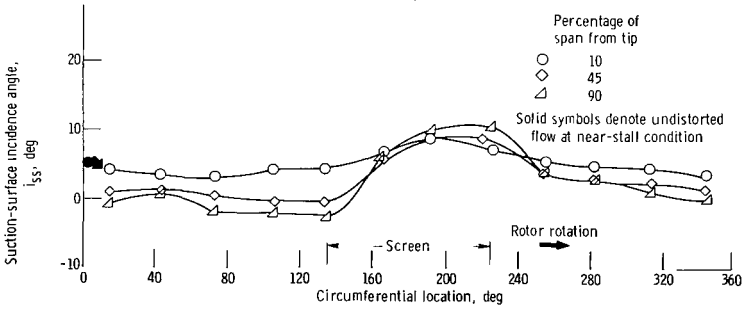

(d) Rotor inlet incidence angle.

Figure 14. - Concluded.

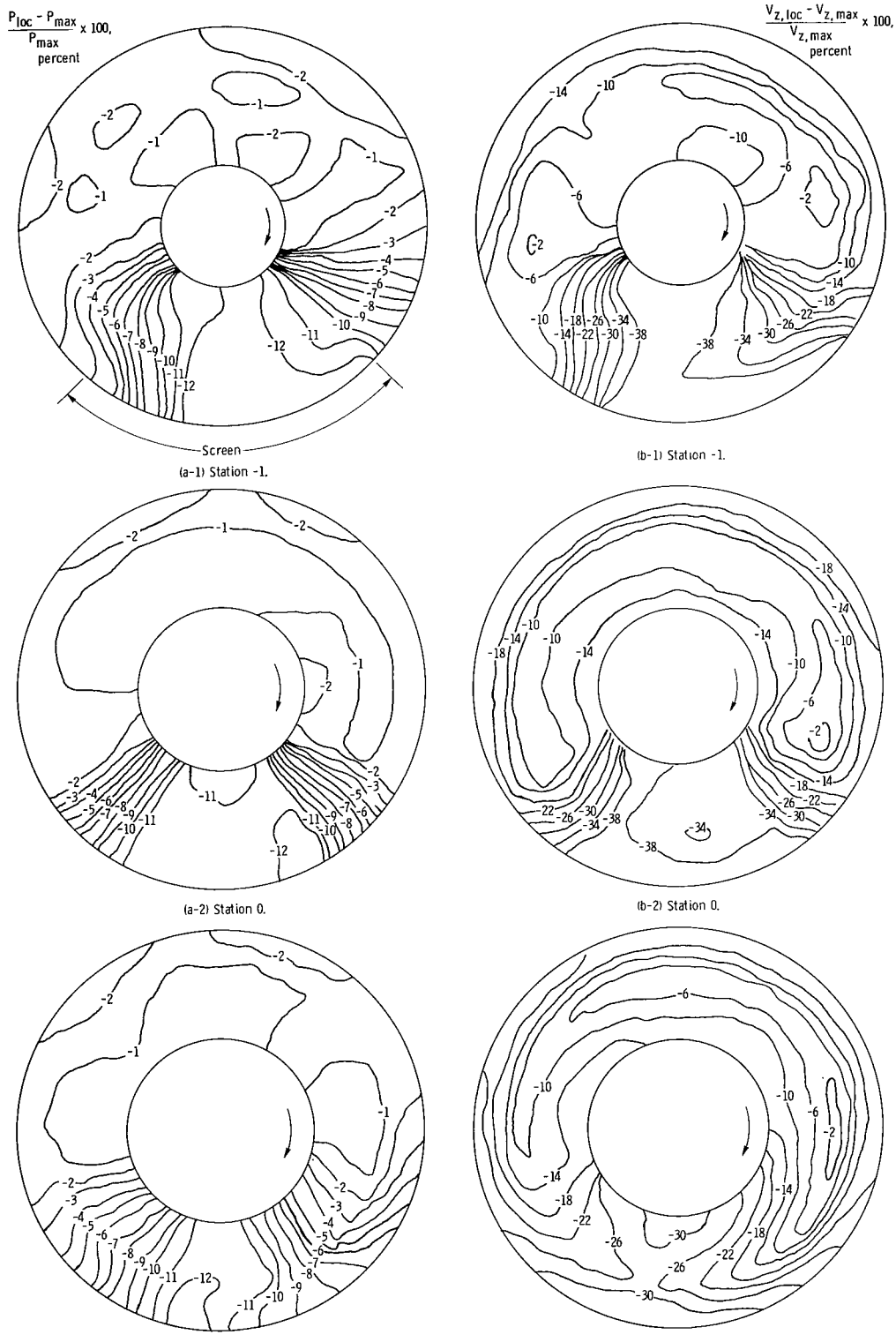

(a-1) Station -1.

(b-1) Station -1.

(a-2) Station 0.

(b-2) Station 0.

(a-3) Station 1 (rotor inlet).

(b-3) Station 1 (rotor inlet).

(a) Total pressure.

(b) Axial velocity.

Figure 15. - Contour maps of upstream distribution of flow parameters at near-stall conditions. 100 Percent of design speed; looking downstream.

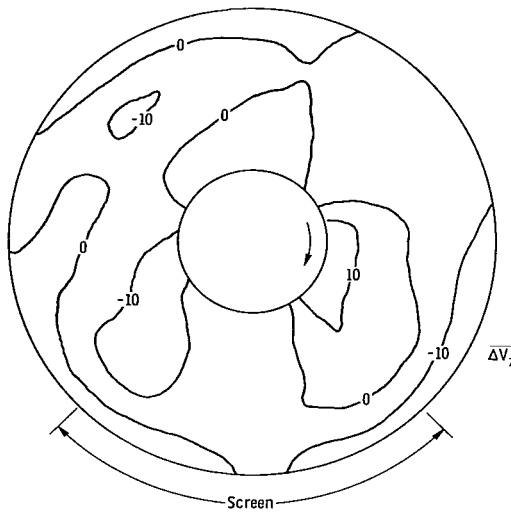

$$\frac{\Delta V_\theta}{\Delta V_z\big|_{\text{Station -1}}} \times 100, \text{ percent}$$

(c-1) Station -1.

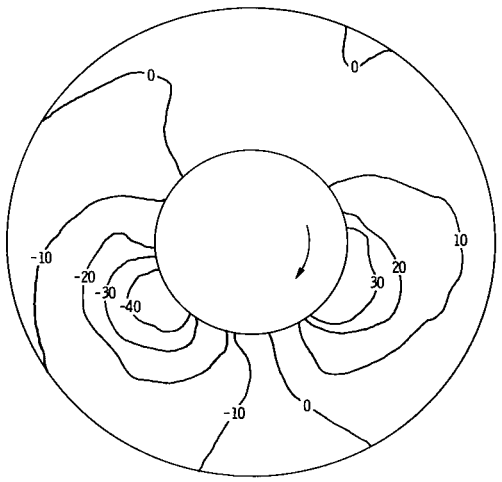

(c-2) Station 0.

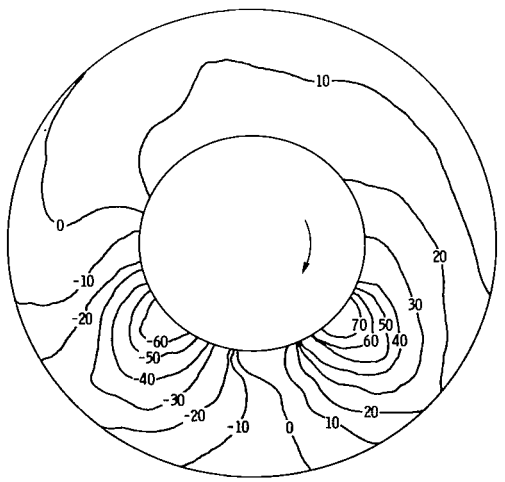

(c-3) Station 1 (rotor inlet).

(c) Absolute tangential velocity.

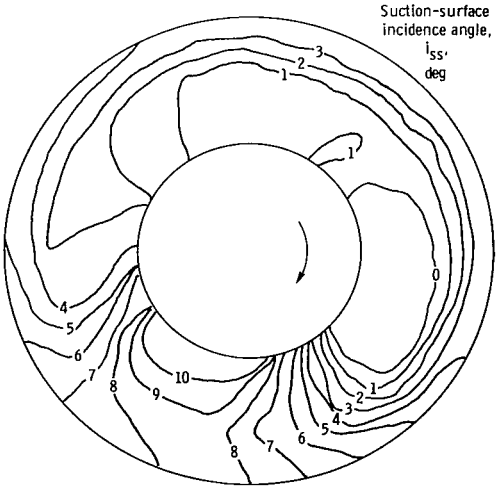

(d) Rotor inlet incidence angle.

Figure 15. - Concluded.

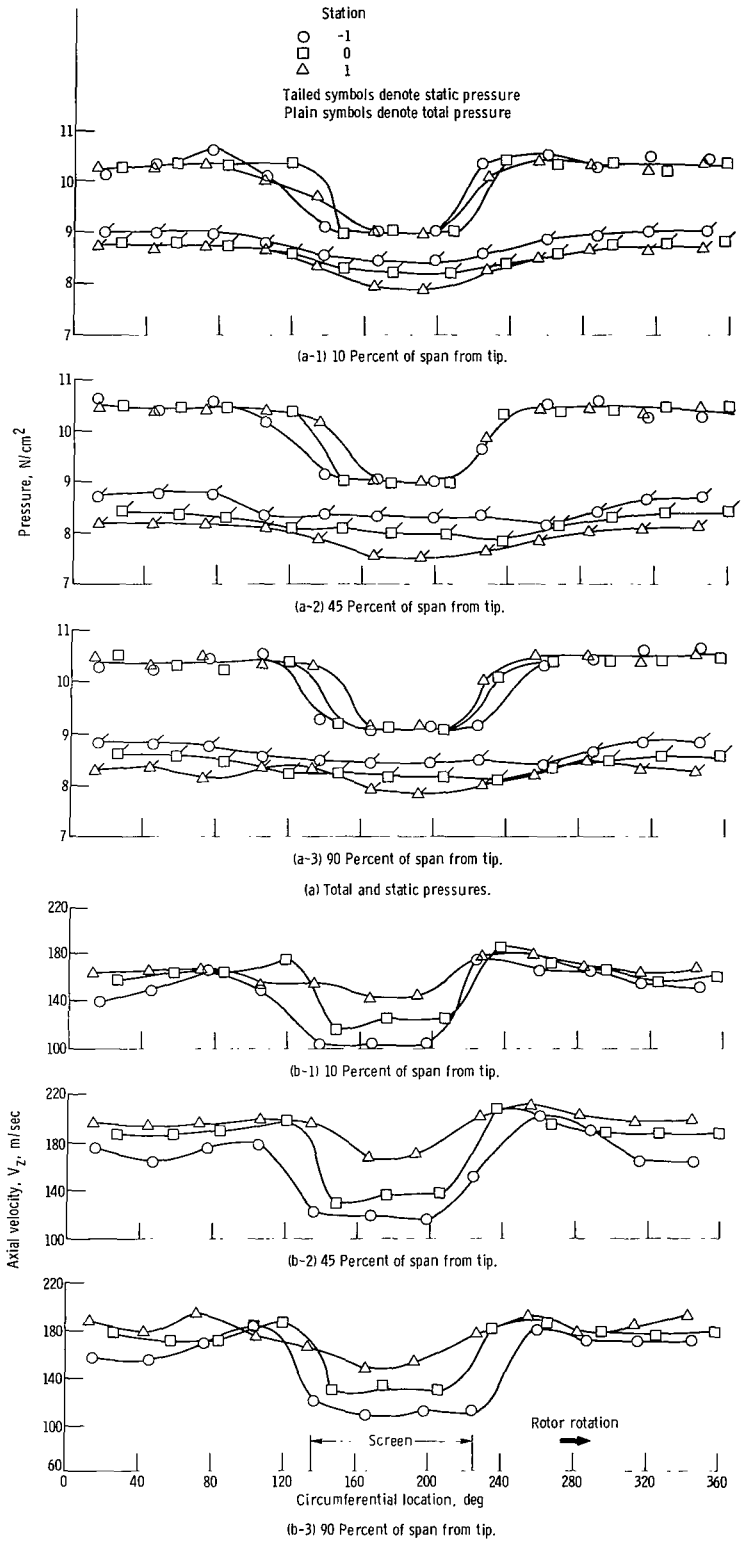

Figure 16. - Circumferential distribution of flow parameters between screen and rotor at maximum-flow conditions. 100 Percent of design speed.

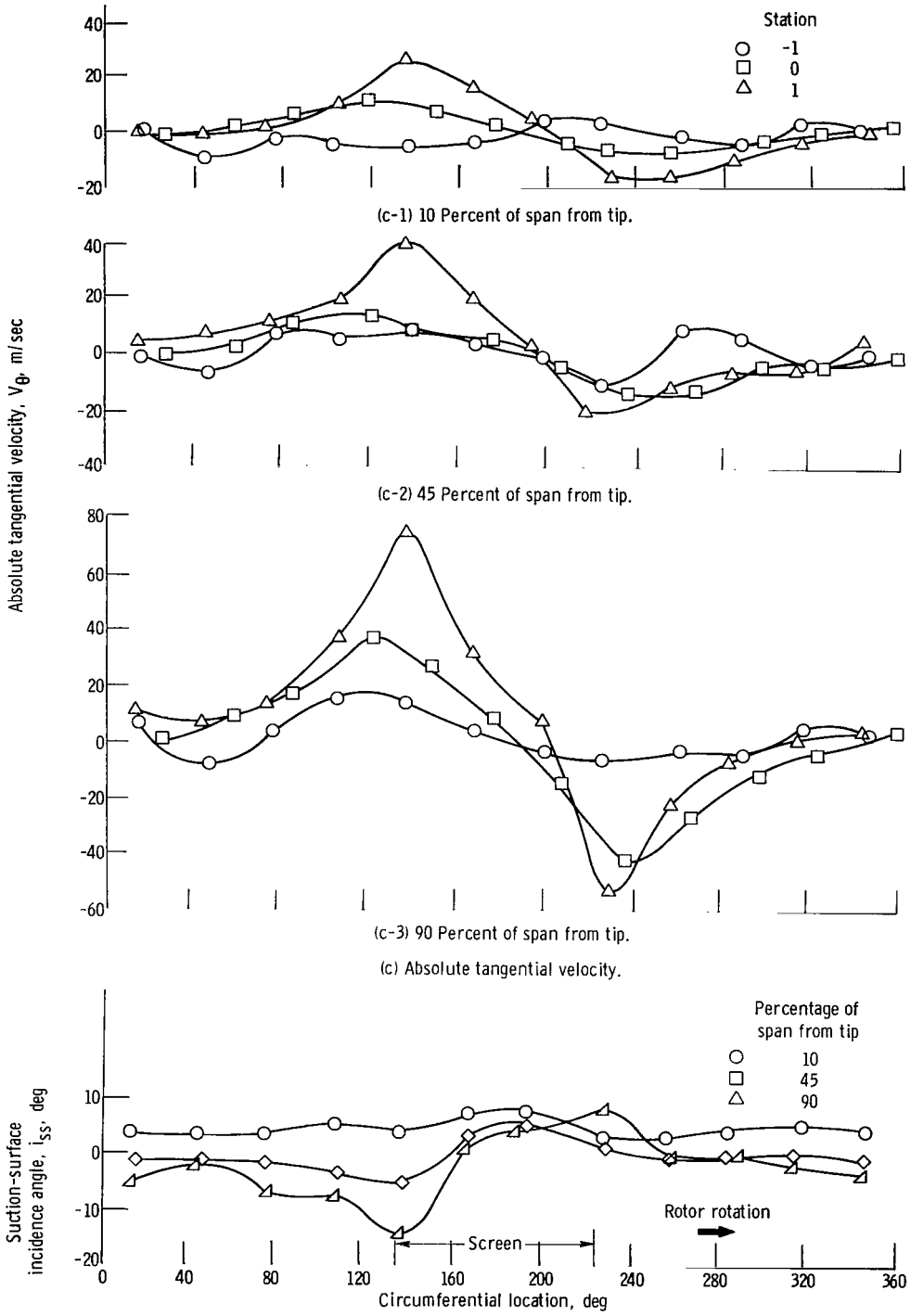

Figure 16. - Concluded.

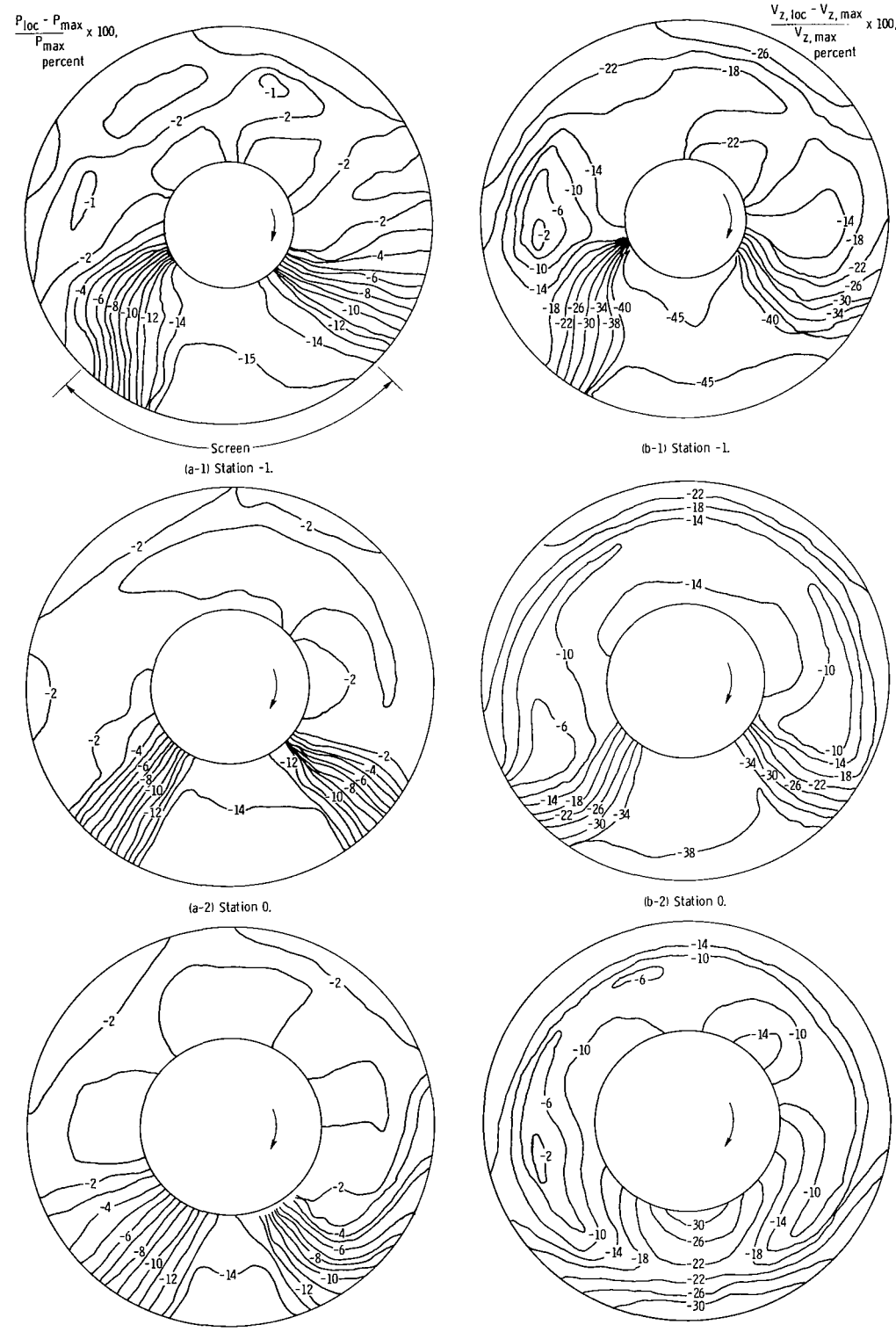

(a-1) Station -1.

(b-1) Station -1.

(a-2) Station 0.

(b-2) Station 0.

(a-3) Station 1 (rotor inlet).

(b-3) Station 1 (rotor inlet).

(a) Total pressure.

(b) Axial velocity.

Figure 17. - Contour maps of upstream distribution of flow parameters at maximum-flow conditions. 100 Percent of design speed; looking downstream.

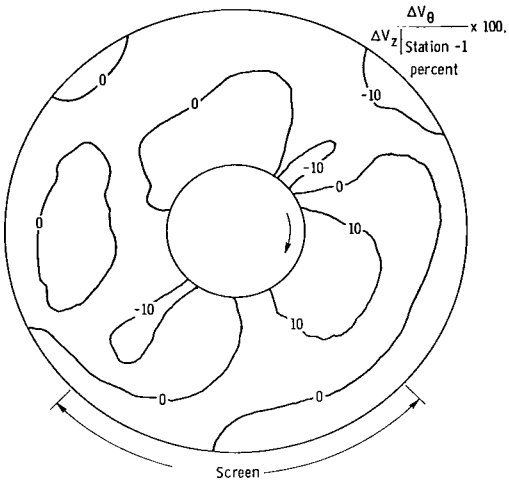

(c-1) Station -1.

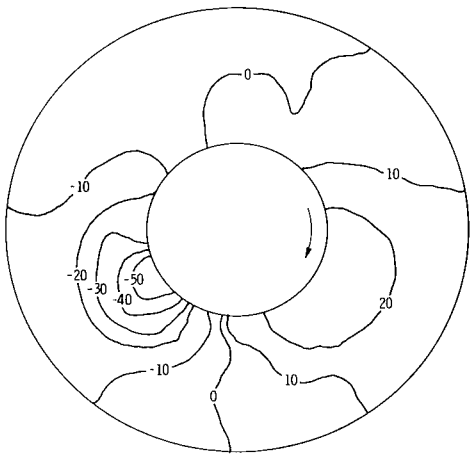

(c-2) Station 0.

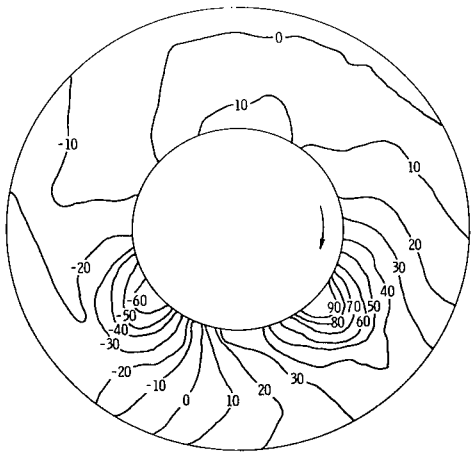

(c-3) Station 1 (rotor inlet).

(c) Absolute tangential velocity.

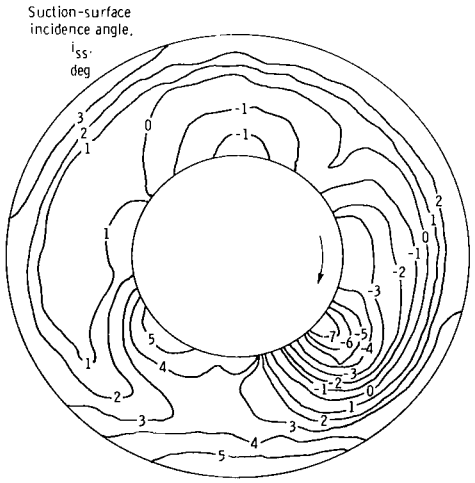

(d) Rotor inlet incidence angle.

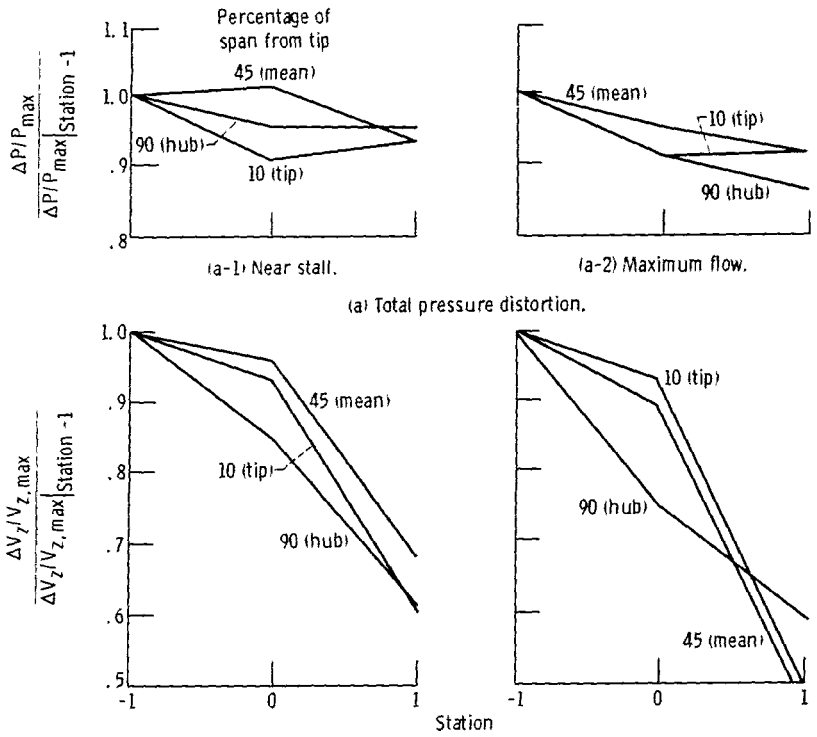

Figure 18. - Upstream attenuation and amplification characteristics of flow parameters. 100 Percent of design speed.

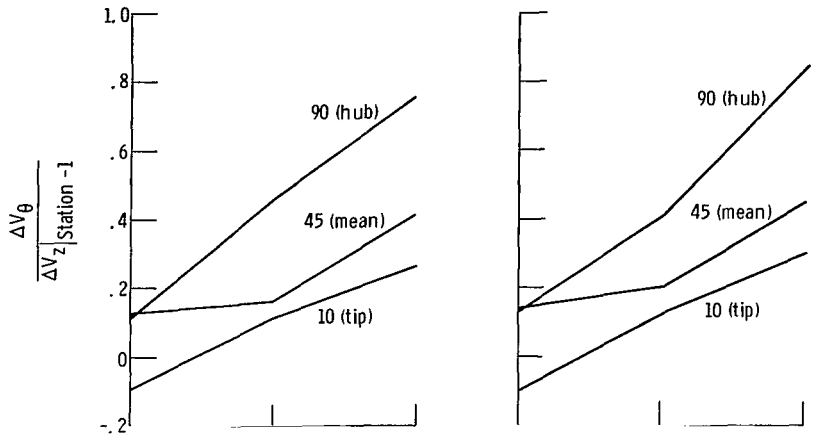

(c-1) Near stall. (c-2) Maximum flow.

(c) Tangential velocity distortion.

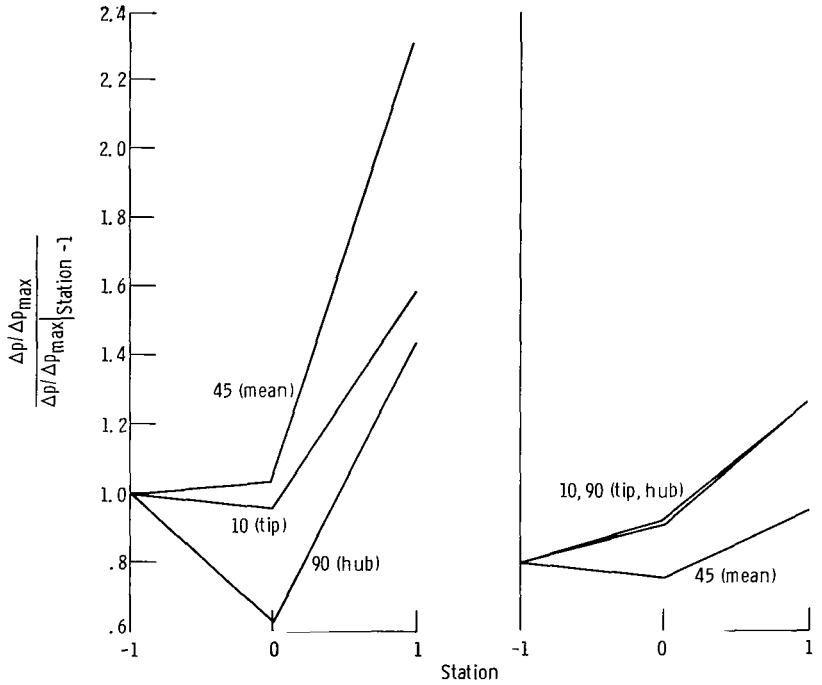

(d-1) Near stall. (d-2) Maximum flow.

(d) Static pressure distortion.

Figure 18. - Concluded.

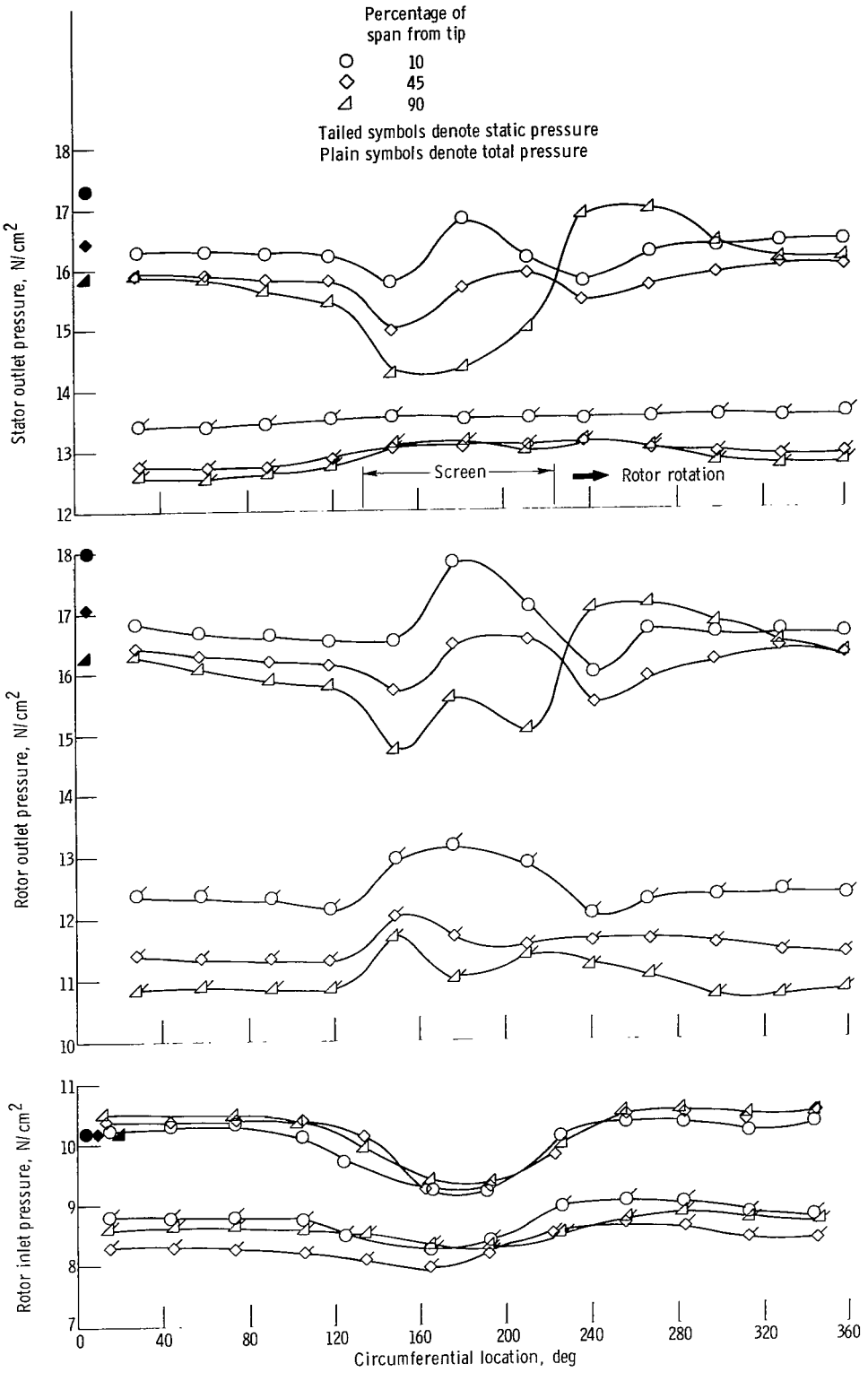

(a) Total and static pressure.

Figure 19. - Circumferential distribution of flow parameters at rotor inlet, rotor outlet, and stator outlet planes at near-stall conditions. 100 Percent of design speed.

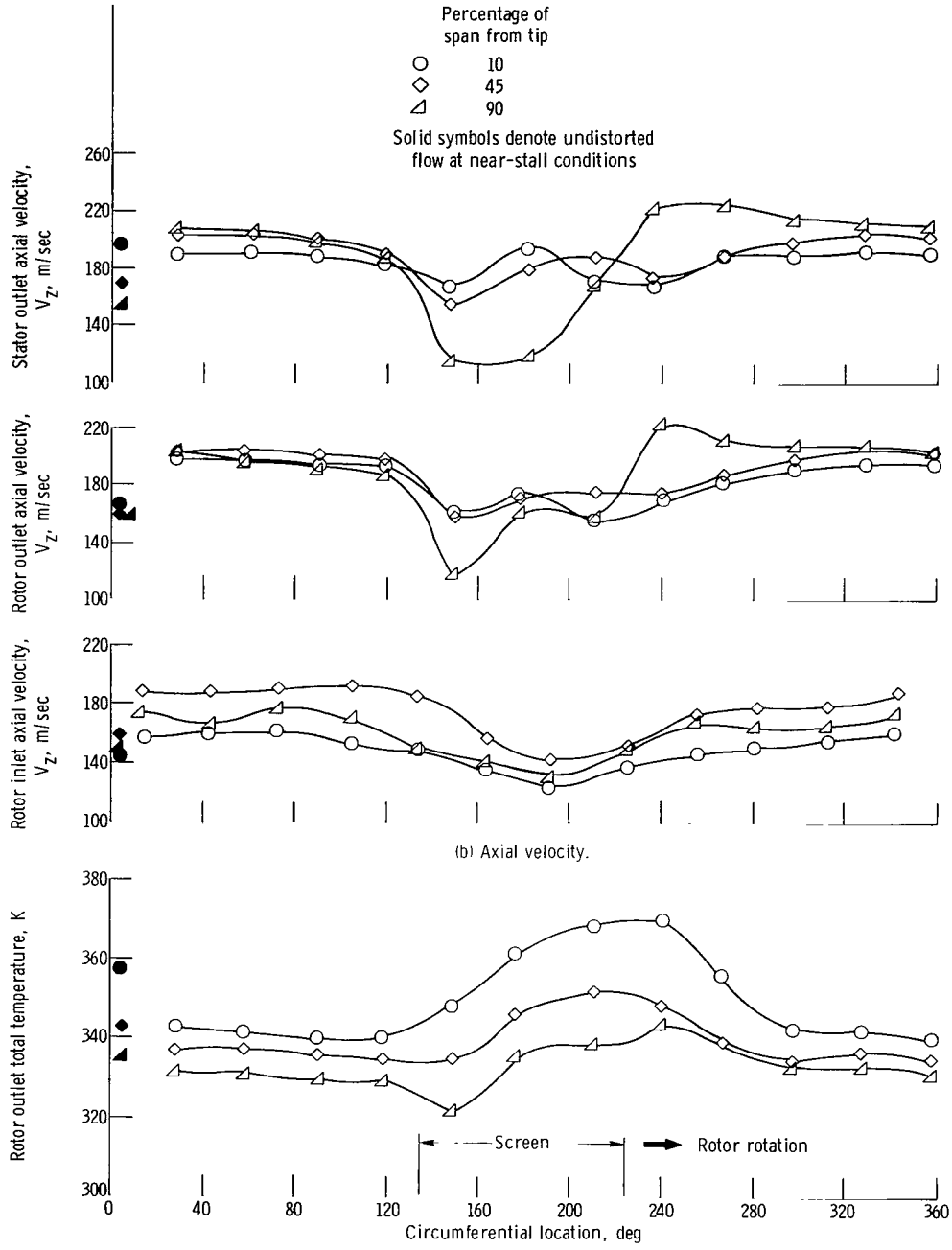

(b) Axial velocity.

(c) Rotor outlet total temperature.

Figure 19. - Continued.

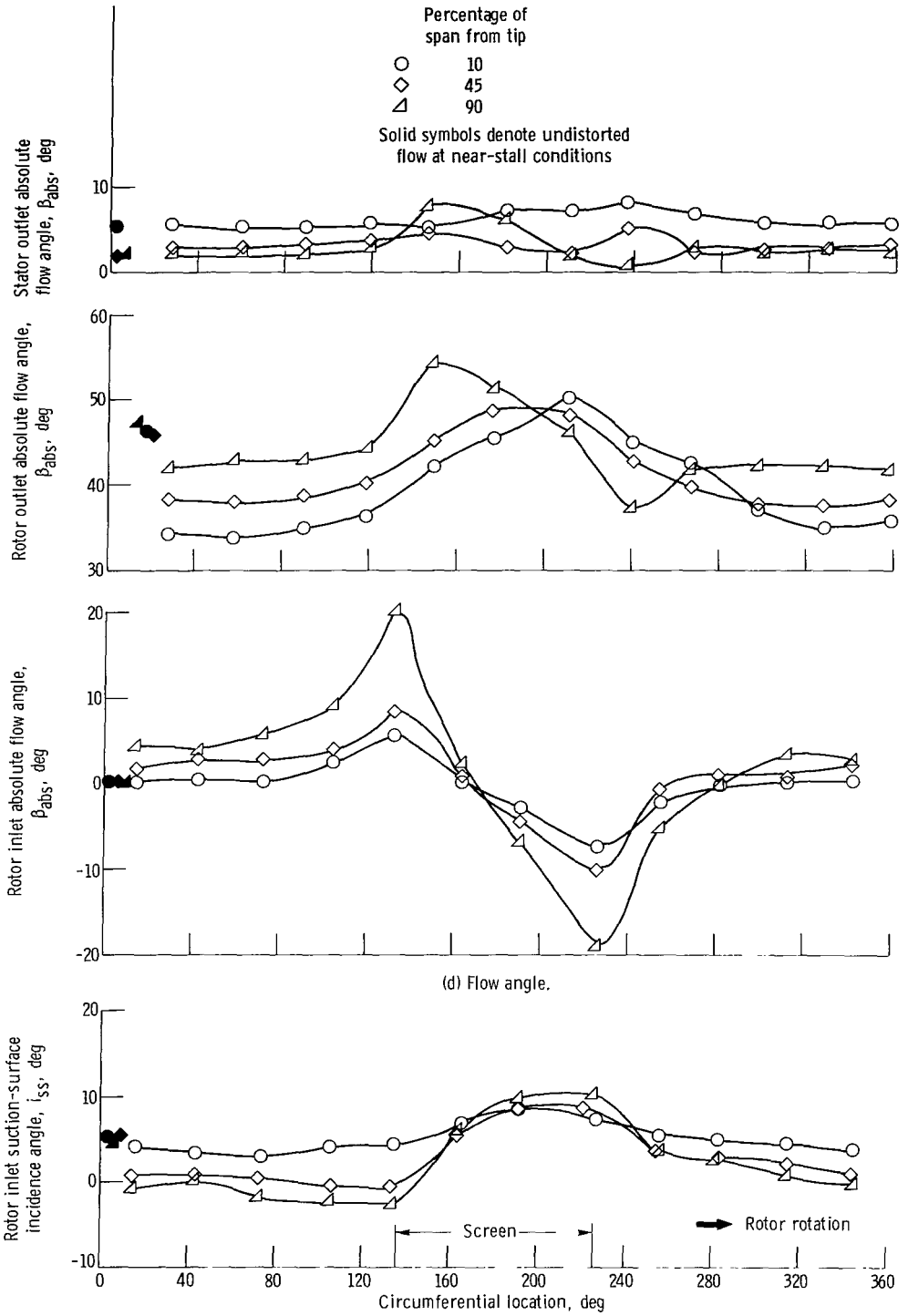

(d) Flow angle.

(e) Rotor inlet incidence angle.

Figure 19. - Continued.

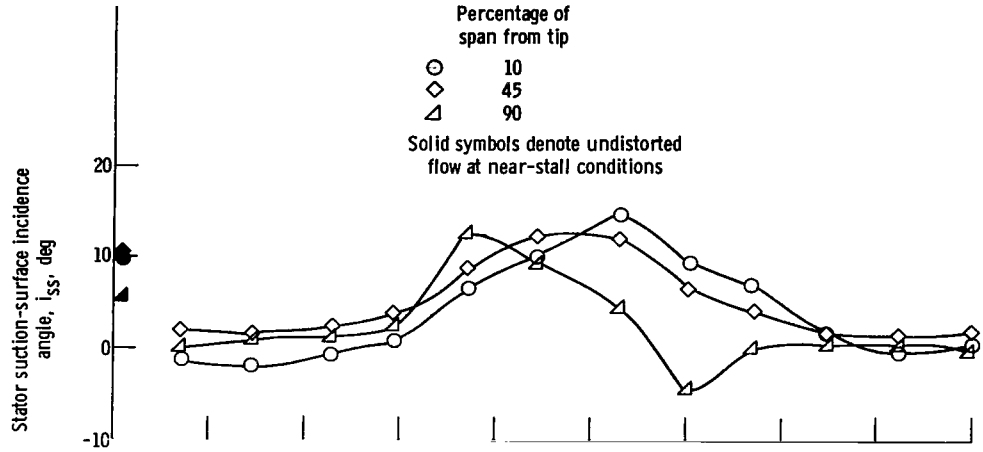

(f) Stator incidence angle.

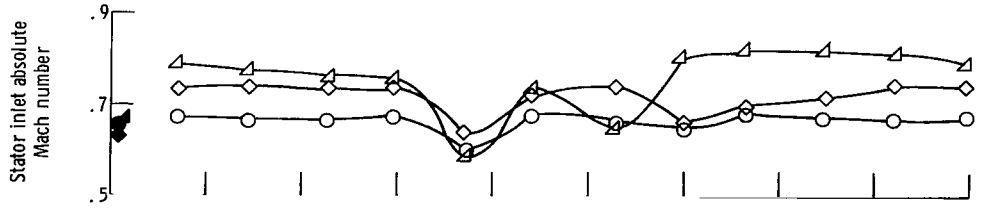

(g) Stator inlet Mach number.

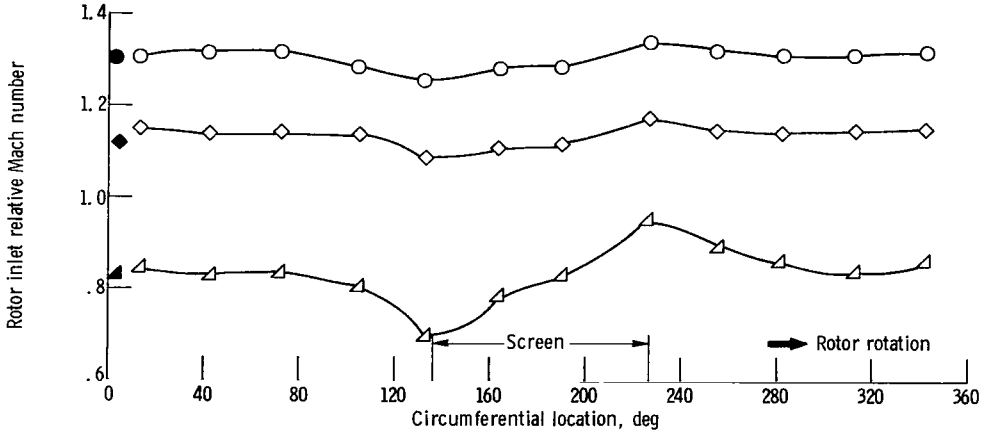

(h) Rotor inlet Mach number.

Figure 19. - Concluded.

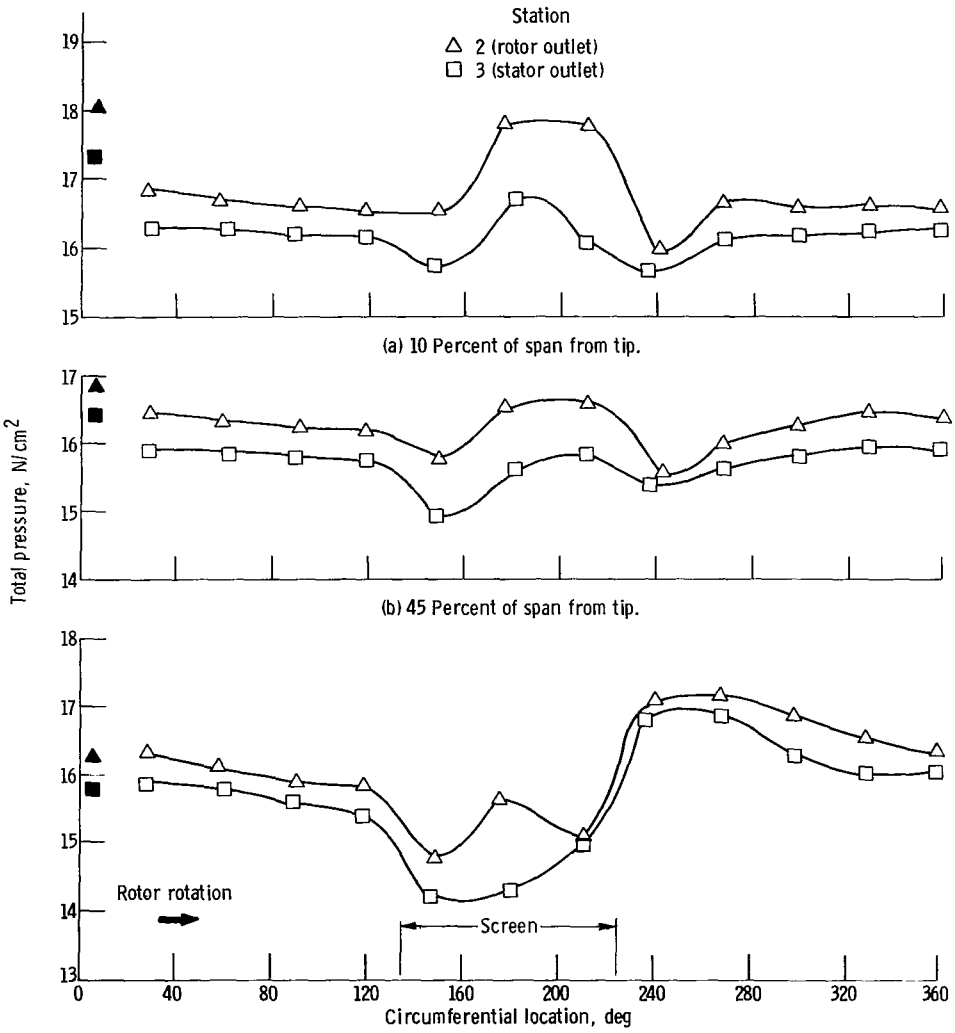

Figure 20. - Circumferential distribution of total pressure at rotor and stator outlet planes. 100 Percent of design speed; near-stall condition.

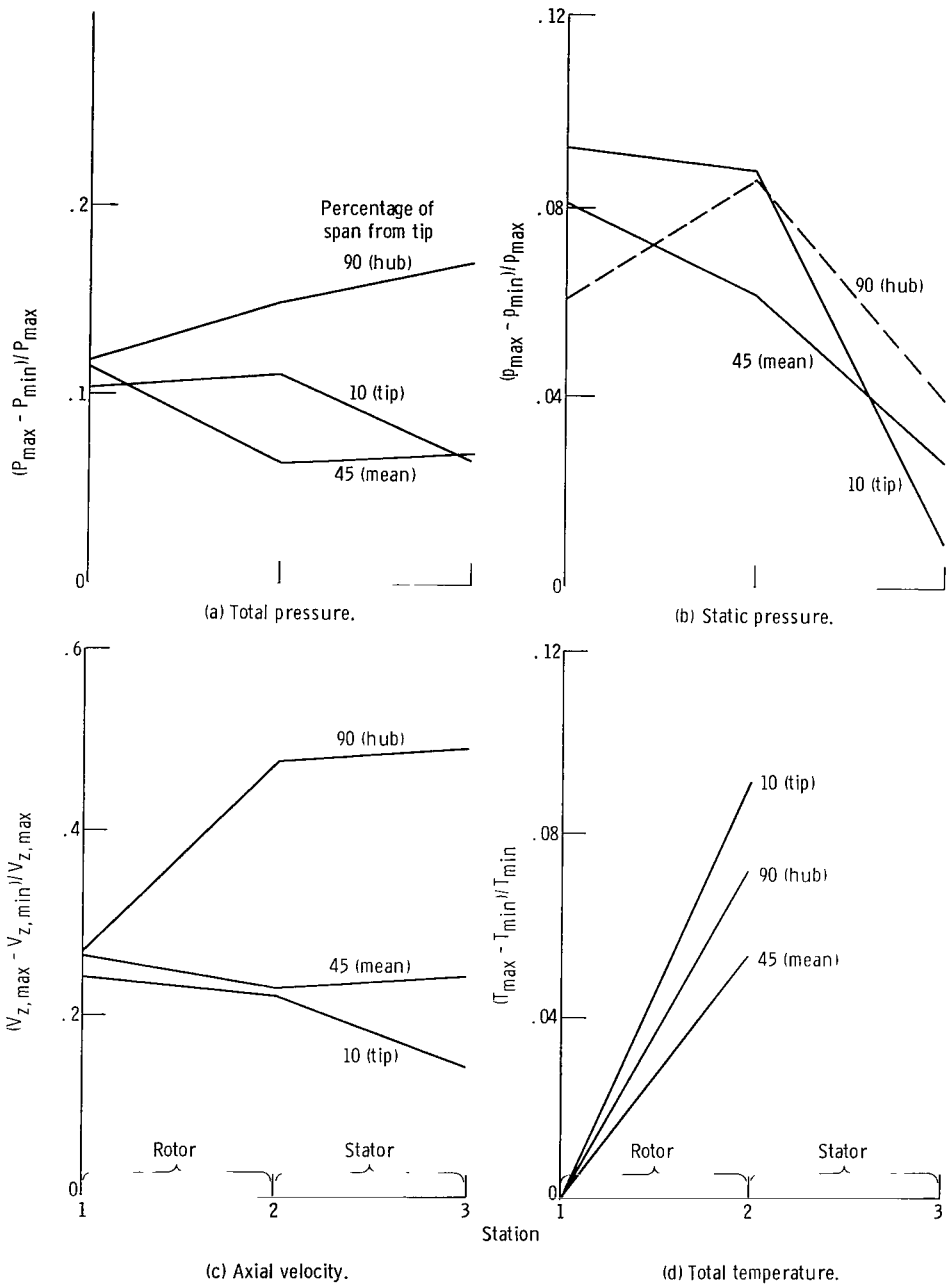

Figure 21. - Attenuation and amplification characteristics of flow parameters for near-stall conditions at 100 percent of design speed.

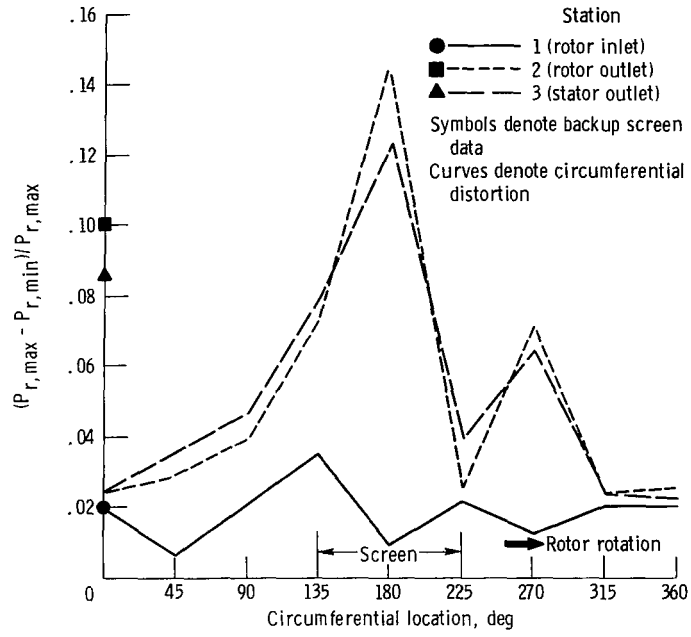

Figure 22. - Radial variations in total pressure due to off-design operation. 100 Percent of design speed; near-stall conditions.

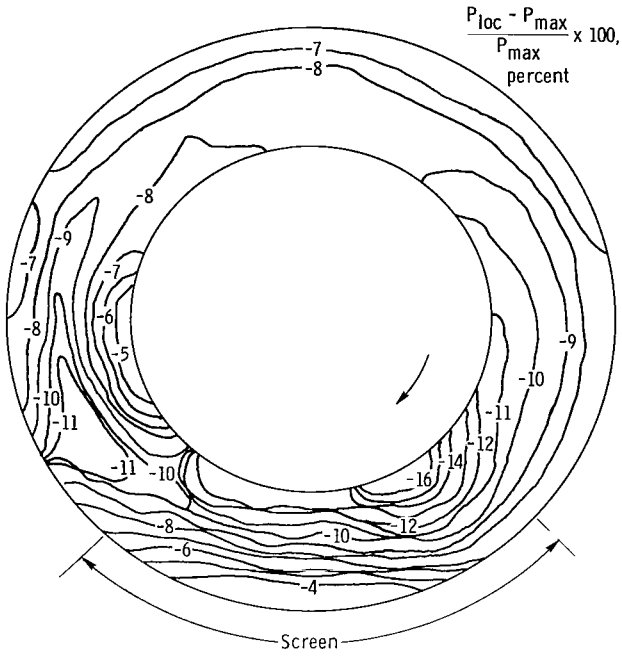

(a) Station 2 (rotor outlet).

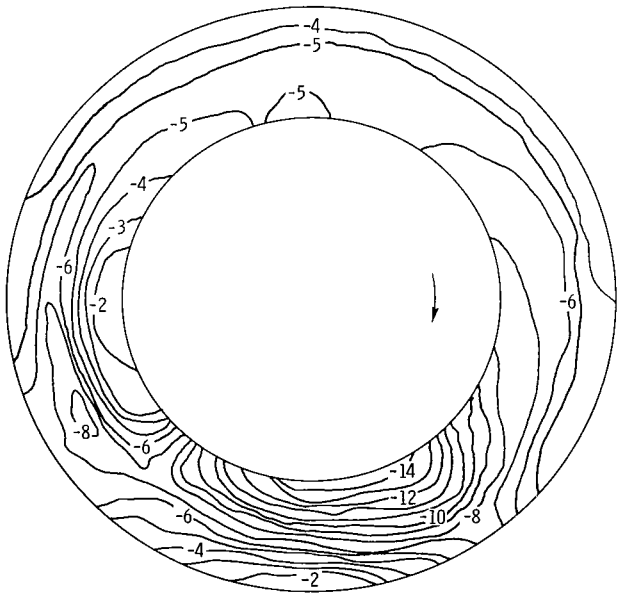

(b) Station 3 (stator outlet).

Figure 23. - Contour maps of distribution of total pressure. 100 Percent of design speed; near-stall condition; looking downstream.

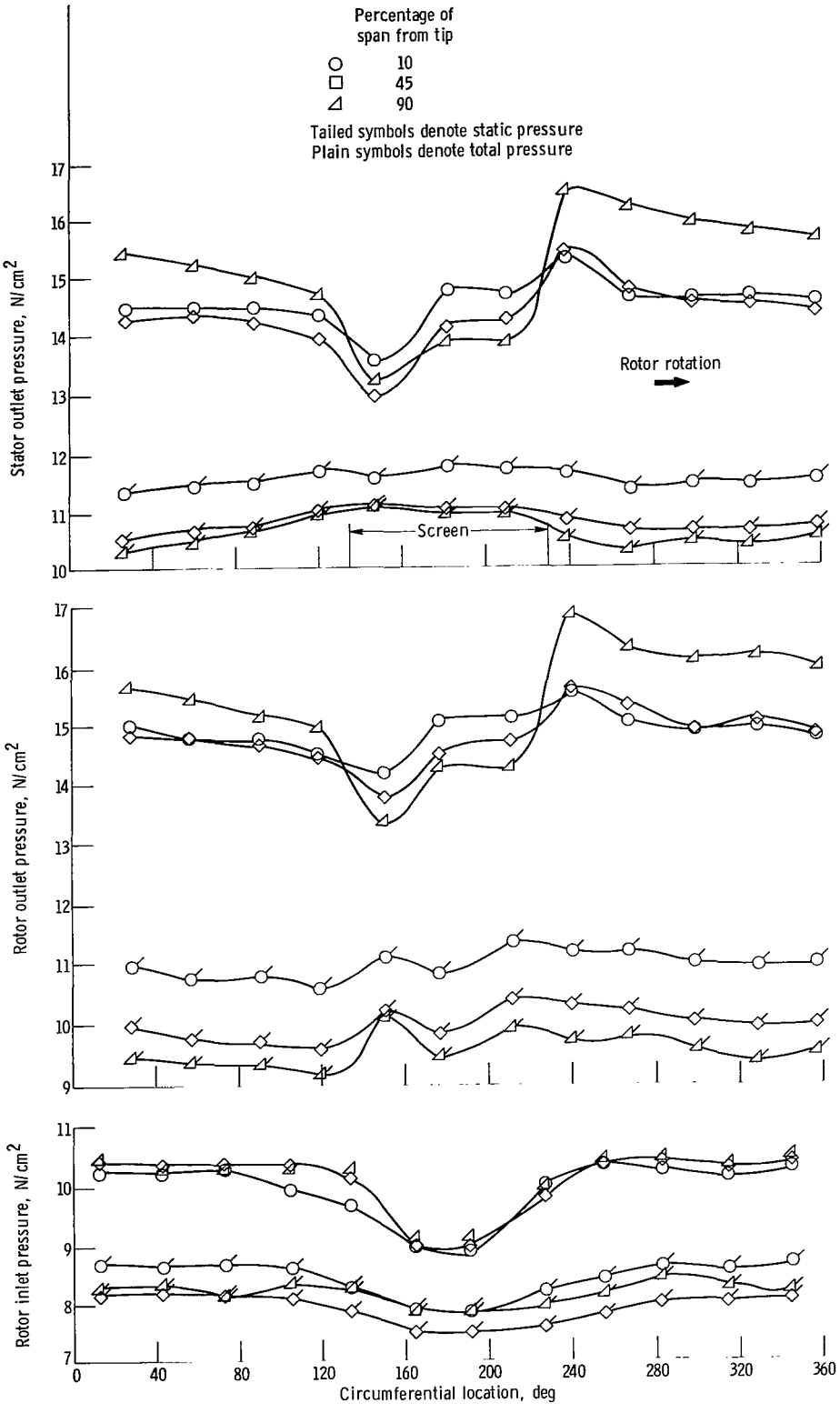

(a) Total and static pressures.

Figure 24. - Circumferential distribution of flow parameters at rotor inlet, rotor outlet, and stator outlet planes at maximum-flow conditions. 100 Percent of design speed.

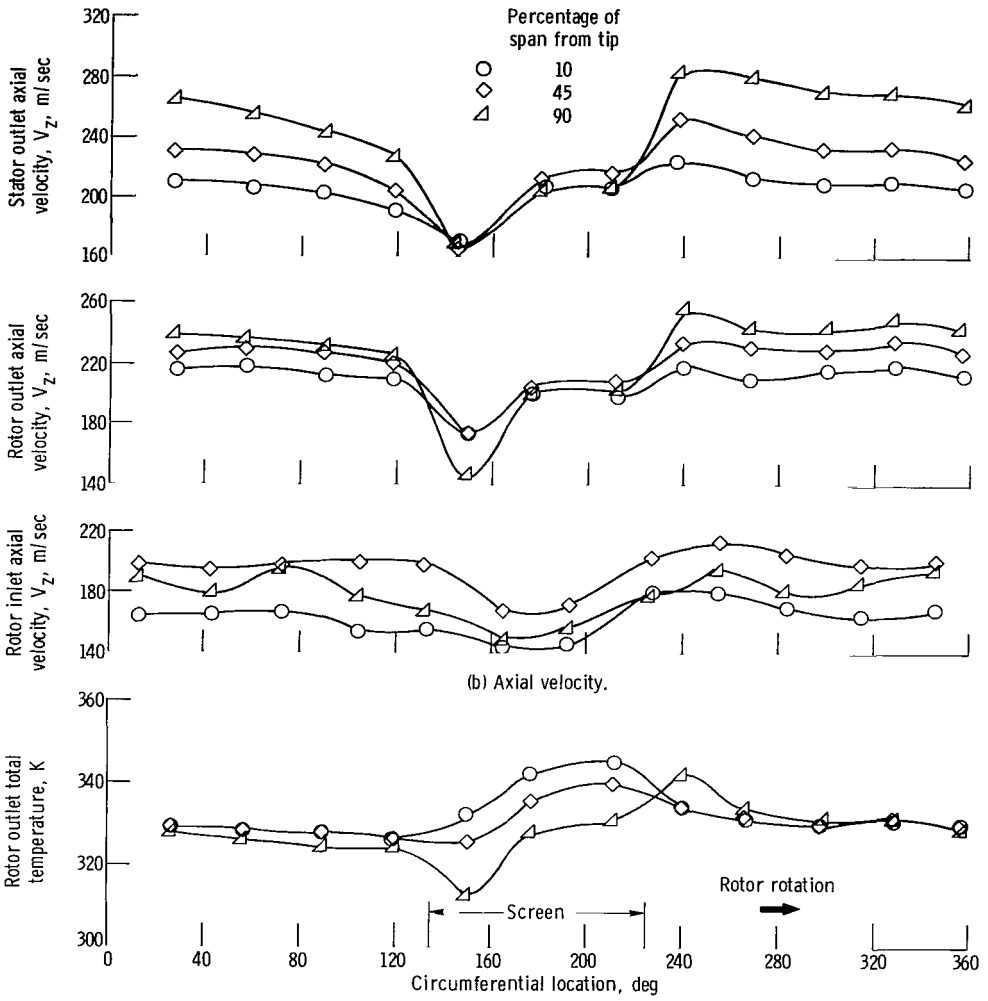

(b) Axial velocity.

(c) Rotor outlet total temperature.

Figure 24. - Continued.

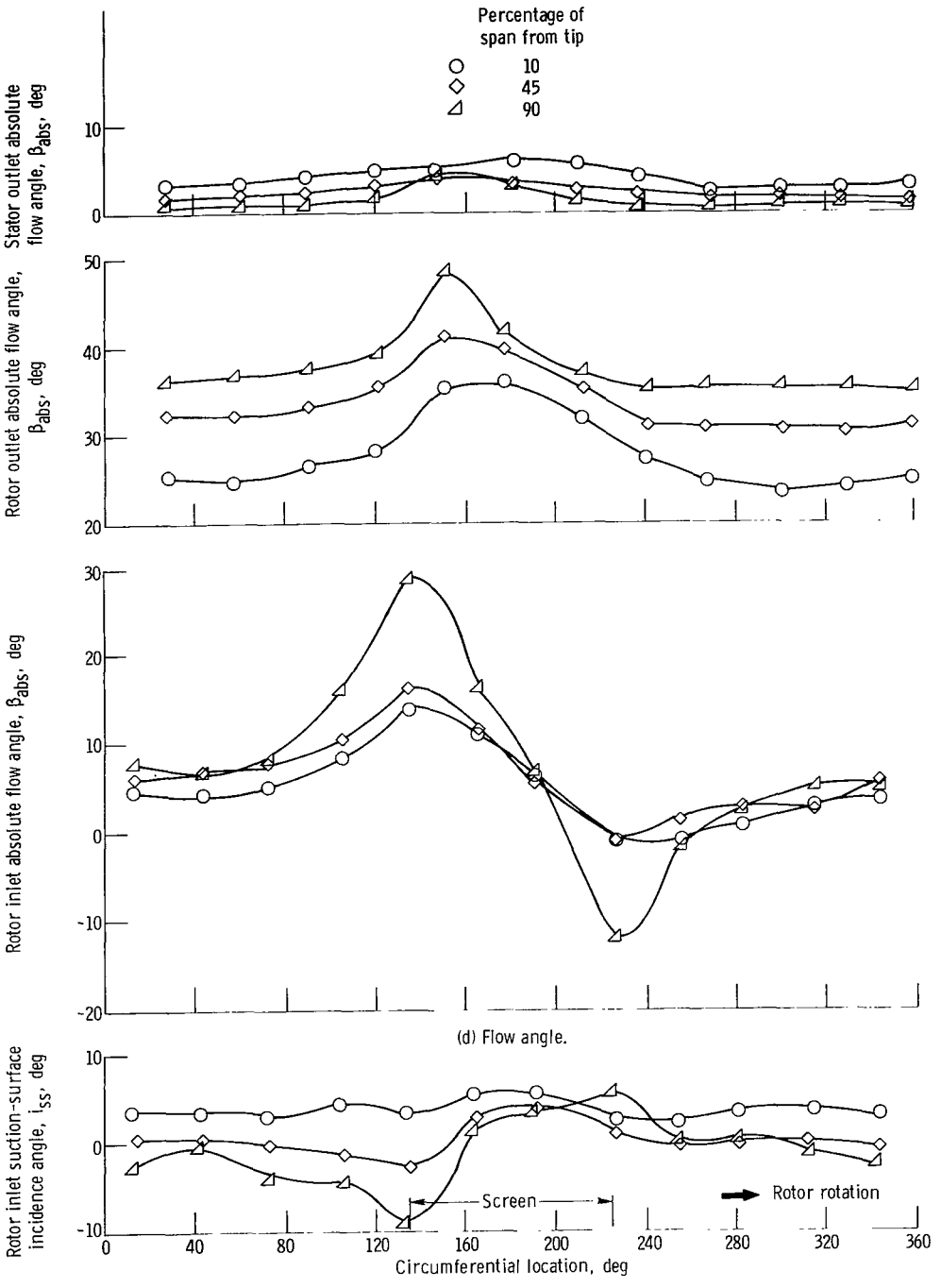

(d) Flow angle.

(e) Rotor inlet incidence angle.

Figure 24. - Continued.

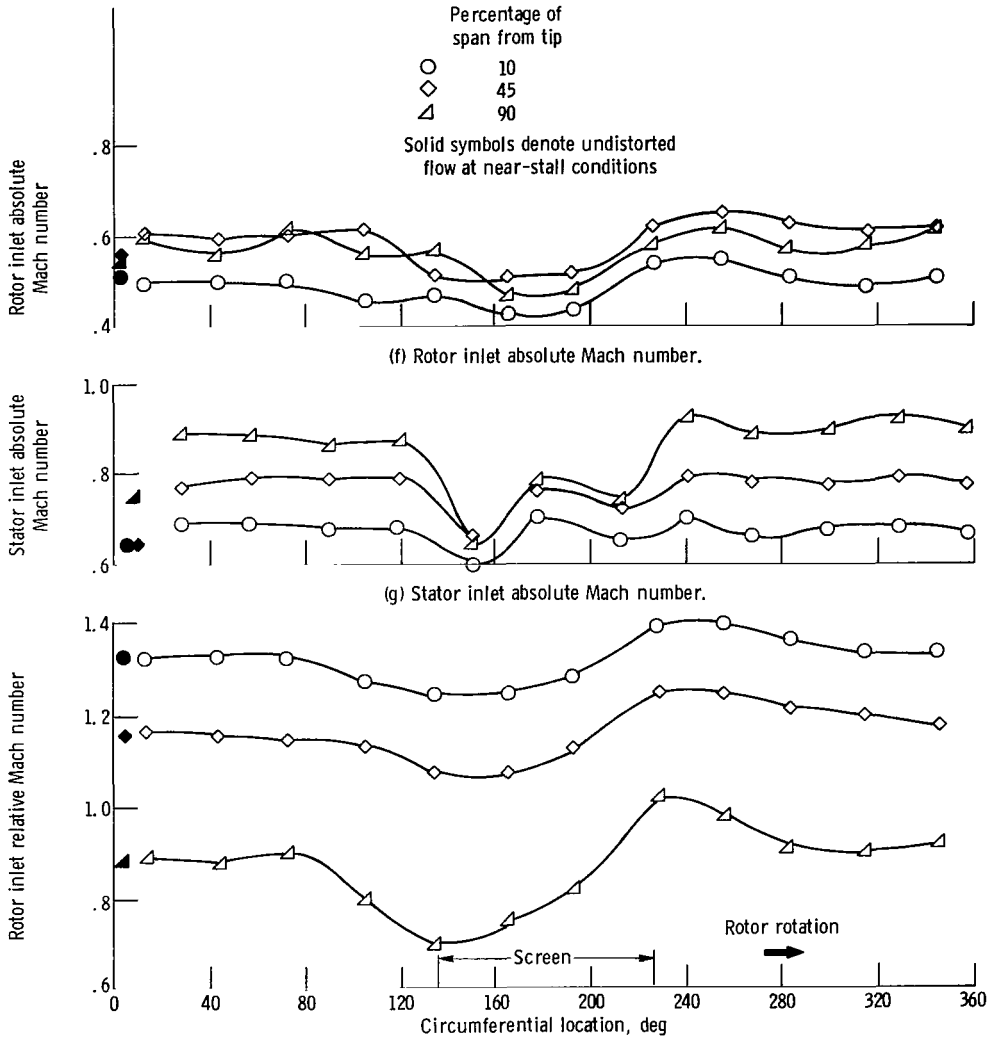

(f) Rotor inlet absolute Mach number.

(g) Stator inlet absolute Mach number.

(h) Rotor inlet relative Mach number.

Figure 24. - Concluded.

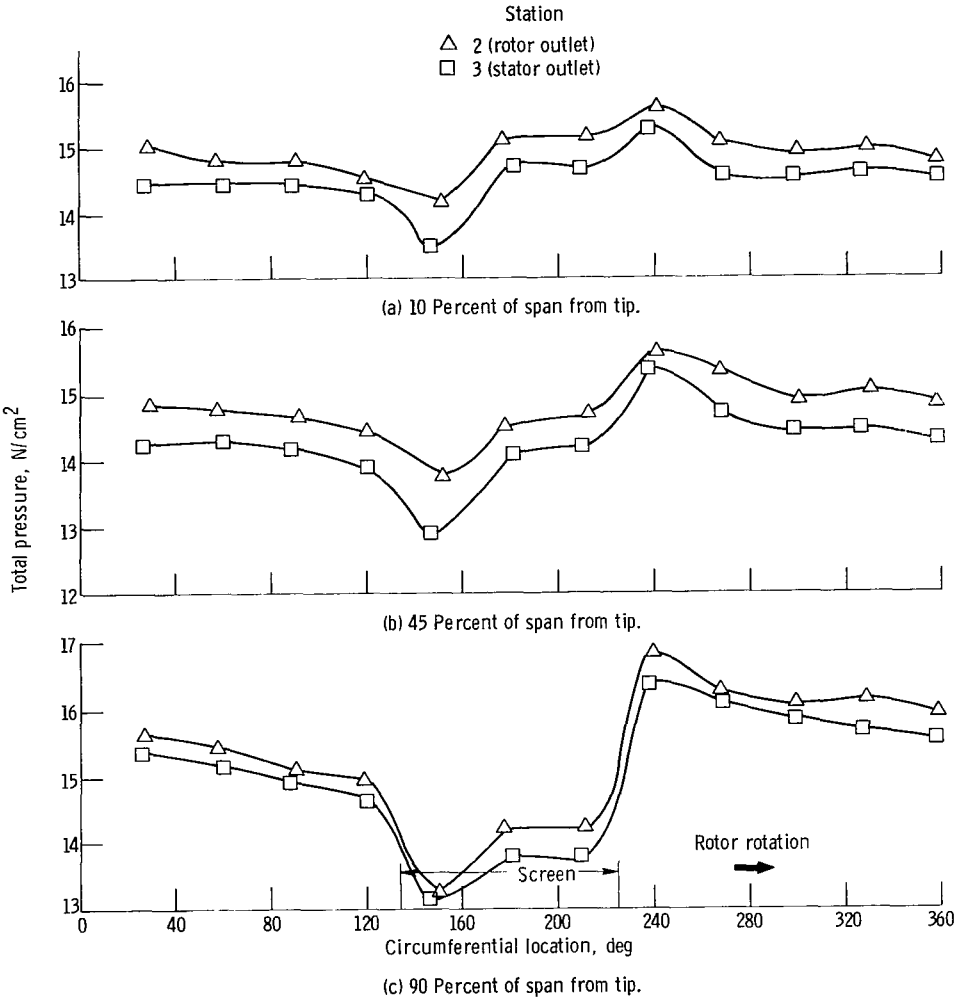

(a) 10 Percent of span from tip.

(b) 45 Percent of span from tip.

(c) 90 Percent of span from tip.

Figure 25. - Total pressures at rotor and stator outlet planes for 100 percent of design speed. Maximum-flow conditions.

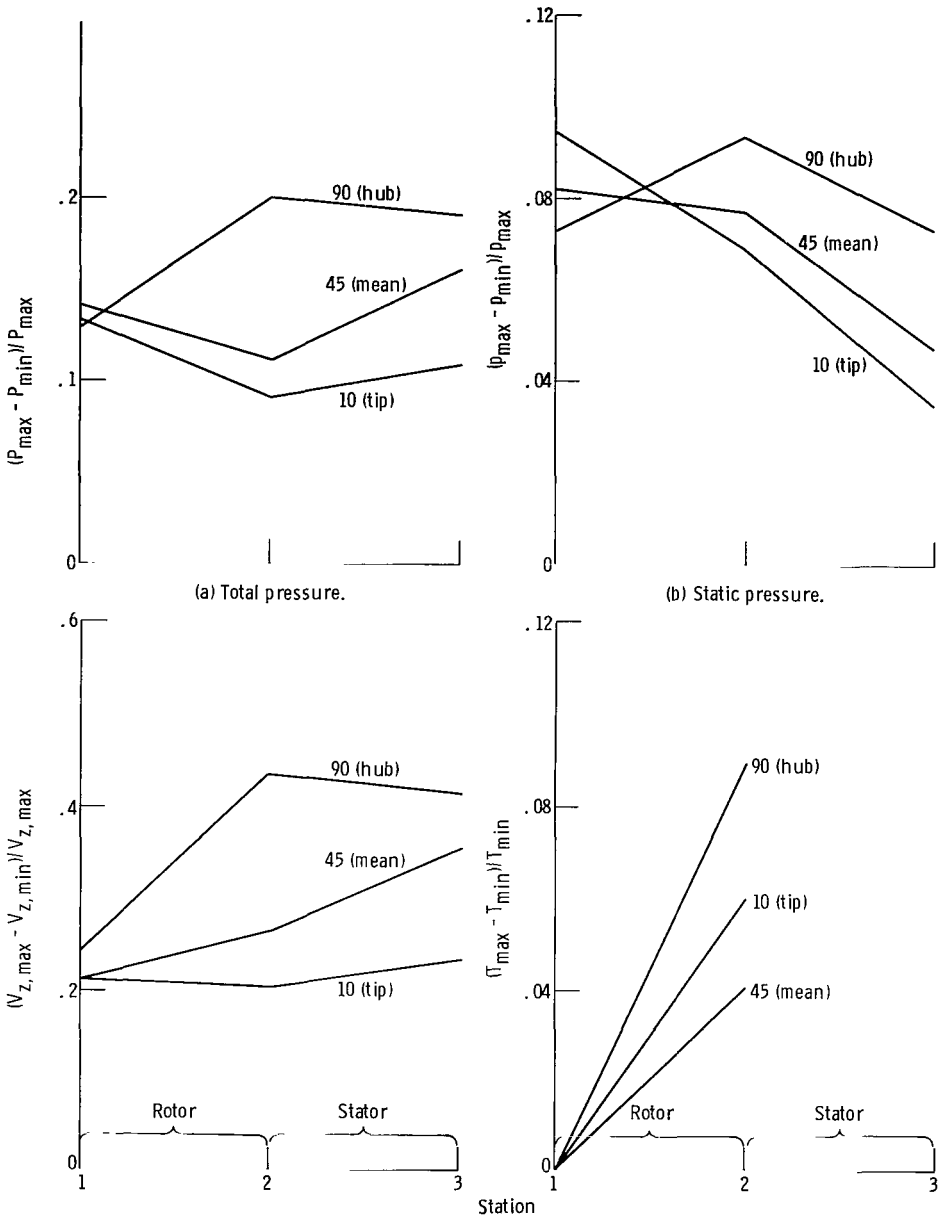

Figure 26. - Attenuation and amplification characteristics of flow parameters for maximum-flow conditions at 100 percent of design speed.

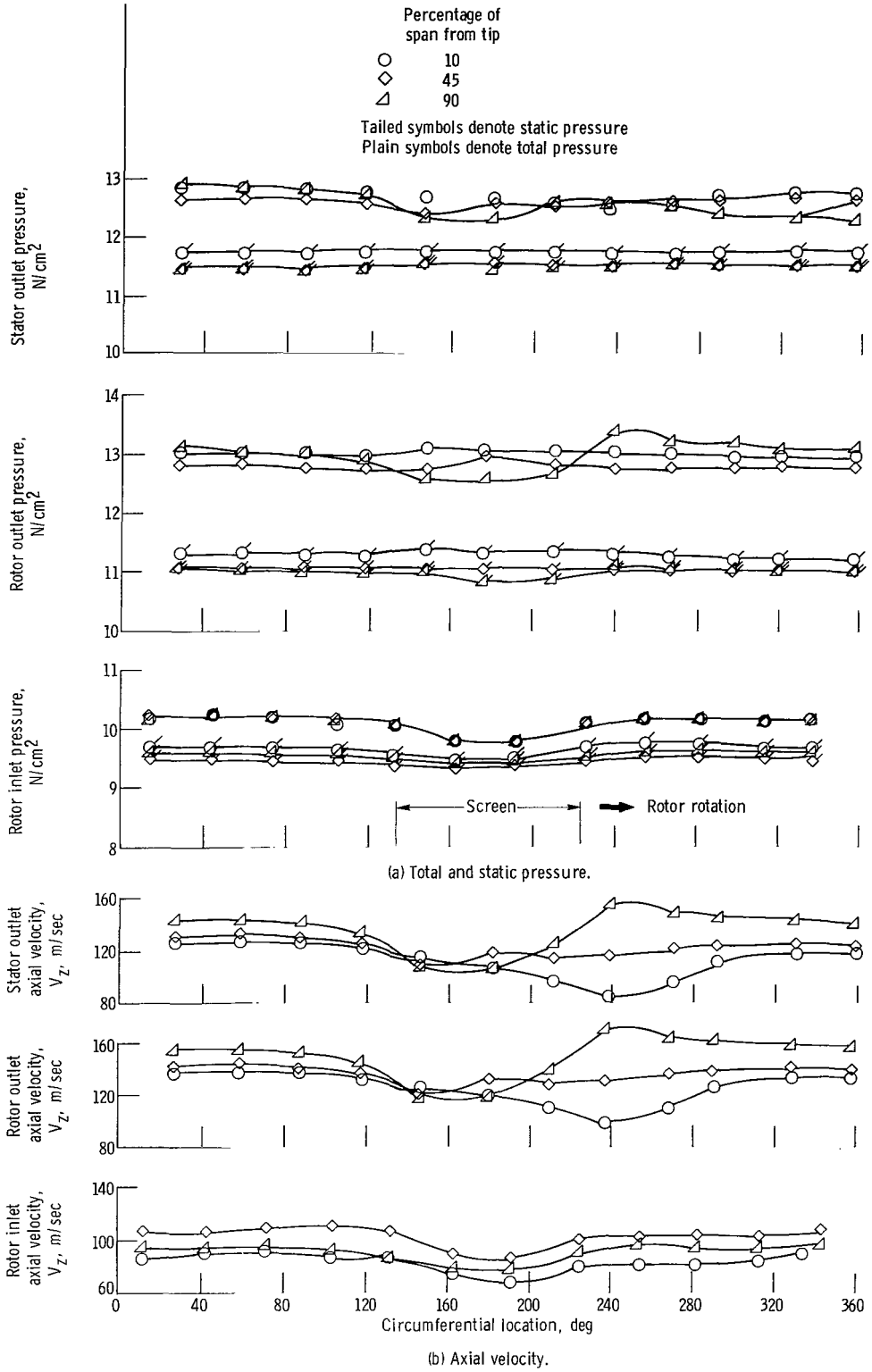

Figure 27. - Circumferential distribution of flow parameters at rotor inlet, rotor outlet, and stator outlet planes at near-stall conditions. 70 Percent of design speed.

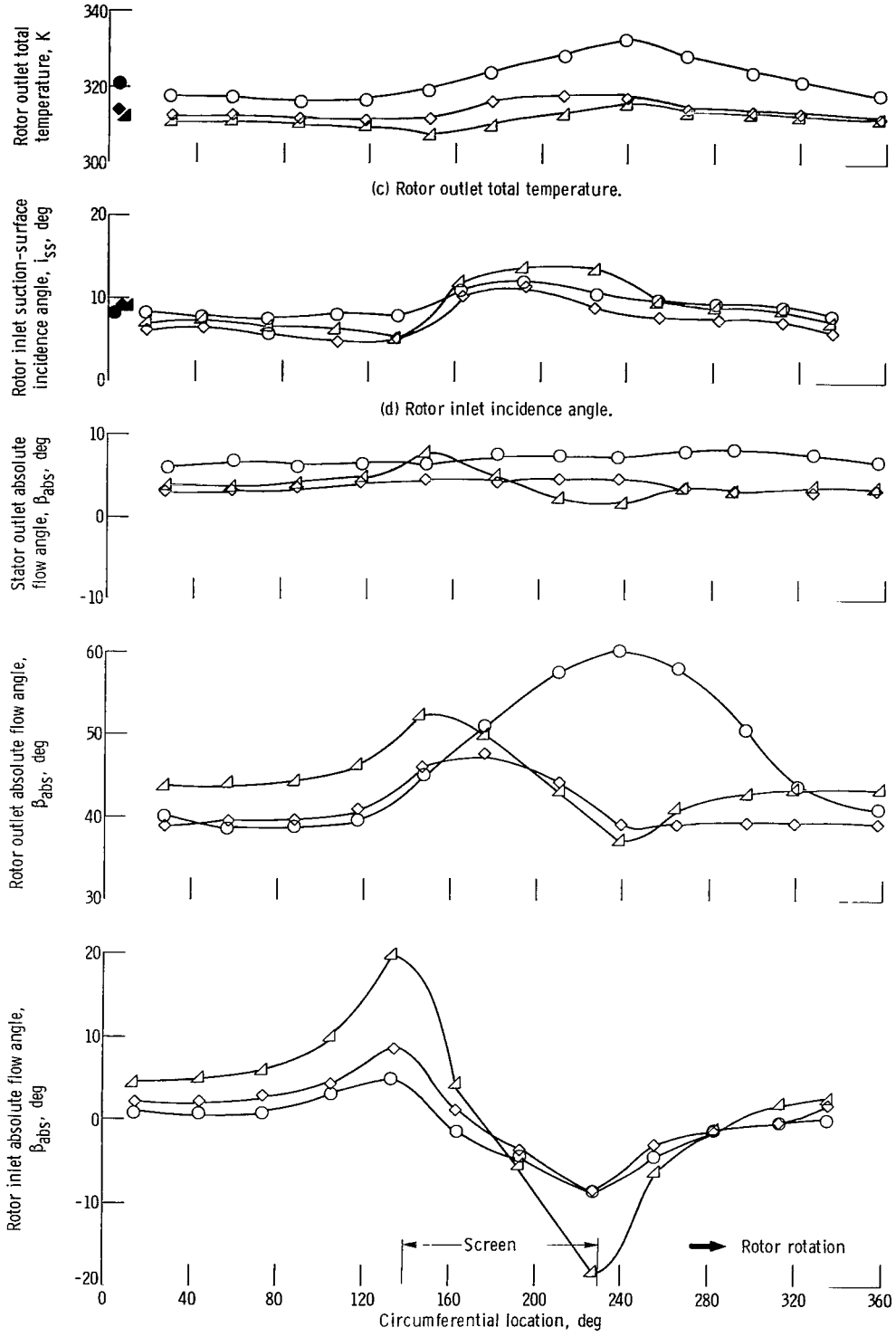

(c) Rotor outlet total temperature.

(d) Rotor inlet incidence angle.

(e) Flow angle.

Figure 27. - Continued.

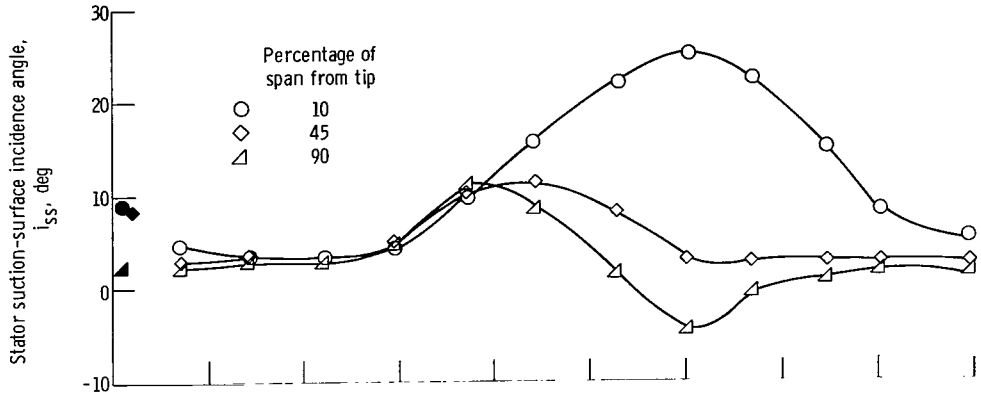

(f) Stator incidence angle.

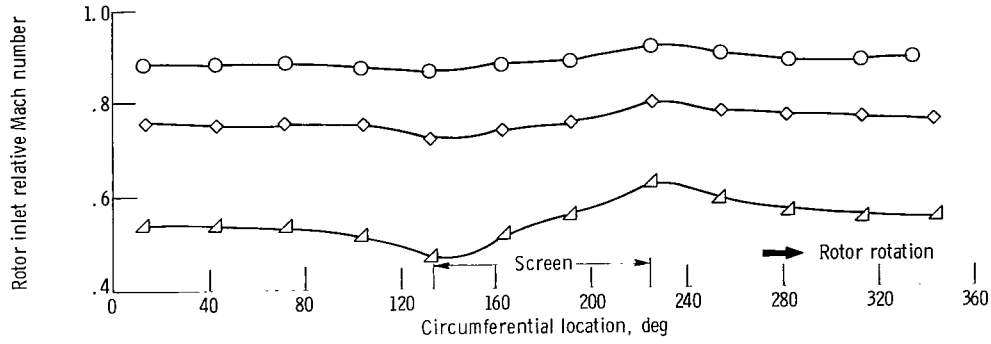

(g) Rotor inlet Mach number.

Figure 27. - Concluded.

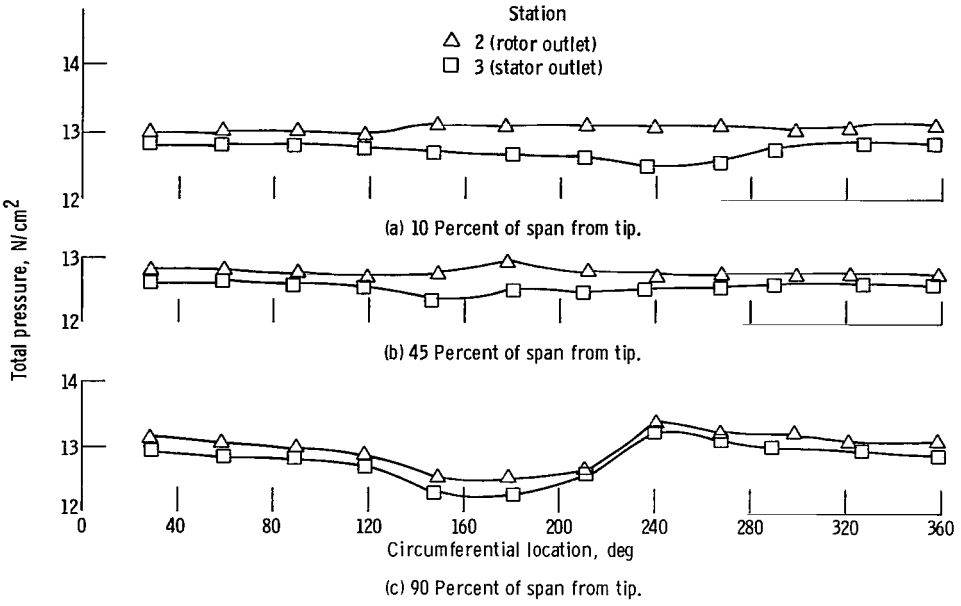

Figure 28. - Total pressures at rotor and stator outlet planes for 70 percent of design speed. Near-stall conditions.

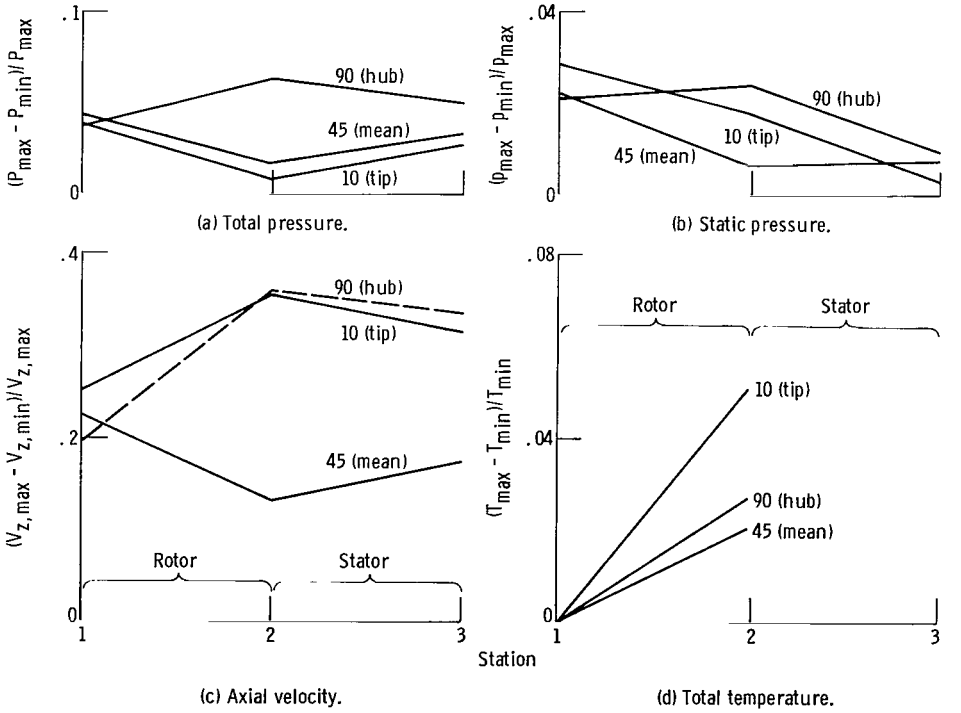

Figure 29. - Attenuation and amplification characteristics of flow parameters for near-stall conditions at 70 percent of design speed.

"The aeronautical and space activities of the United States shall be conducted so as to contribute . . . to the expansion of human knowledge of phenomena in the atmosphere and space. The Administration shall provide for the widest practicable and appropriate dissemination of information concerning its activities and the results thereof."

—NATIONAL AERONAUTICS AND SPACE ACT OF 1958

NASA SCIENTIFIC AND TECHNICAL PUBLICATIONS

TECHNICAL REPORTS: Scientific and technical information considered important, complete, and a lasting contribution to existing knowledge.

TECHNICAL NOTES: Information less broad in scope but nevertheless of importance as a contribution to existing knowledge.

TECHNICAL MEMORANDUMS: Information receiving limited distribution because of preliminary data, security classification, or other reasons. Also includes conference proceedings with either limited or unlimited distribution.

CONTRACTOR REPORTS: Scientific and technical information generated under a NASA contract or grant and considered an important contribution to existing knowledge.

TECHNICAL TRANSLATIONS: Information published in a foreign language considered to merit NASA distribution in English.

SPECIAL PUBLICATIONS: Information derived from or of value to NASA activities. Publications include final reports of major projects, monographs, data compilations, handbooks, sourcebooks, and special bibliographies.

TECHNOLOGY UTILIZATION PUBLICATIONS: Information on technology used by NASA that may be of particular interest in commercial and other non-aerospace applications. Publications include Tech Briefs, Technology Utilization Reports and Technology Surveys.

Details on the availability of these publications may be obtained from:

SCIENTIFIC AND TECHNICAL INFORMATION OFFICE

NATIONAL AERONAUTICS AND SPACE ADMINISTRATION

Washington, D.C. 20546